Numerical Study on Punching Shear Responses of Flat Plate Structures Strengthened with Engineered Cementitious Composites

Alina Serik, B. Eng

Submitted in fulfillment of the requirements
for the degree of Master of Science
in Civil & Environmental Engineering

School of Engineering and Digital Sciences
Department of Civil & Environmental Engineering
Nazarbayev University

53 Kabanbay Batyr Avenue, Astana, Kazakhstan, 010000

Supervisors: Dichuan Zhang, Jong Kim

Date of completion: April, 2024

Declaration

I hereby, declare that this manuscript, entitled “Numerical study on punching shear responses of flat plate structures strengthened with engineered cementitious composites”, is the result of my own work except for quotations and citations which have been duly acknowledged.

I also declare that, to the best of my knowledge and belief, it has not been previously or concurrently submitted, in whole or in part, for any other degree or diploma at Nazarbayev University or any other national or international institution.

Name: Alina Serik

Date: April 5, 2024

Abstract

Flat plates are one of the conventional structural systems found in the construction sector due to their several advantages including simplicity, lowered expenses, and architectural mobility. However, the flat plate systems are vulnerable to punching shear failures which happen suddenly and catastrophically. Thus, it is crucial to develop strengthening techniques to augment the punching shear resistance of such structures. The strengthening techniques include shear reinforcement, drop panels, and column capital. One of the modern techniques for retrofitting flat plates is the use of engineered cementitious composites (ECC), applied as thin layers on both sides of slab surfaces. There are only limited studies that examined the response of flat plates with ECC retrofitting that improved the punching shear resistance. Most previous research has employed experimental methods to assess the impact of ECC on the punching shear capacity of the slab considering limited design parameters due to economic constraints. Furthermore, some inconsistent results were reported from two separate studies. In one study, the tension side retrofitting with ECC showed a noticeable contribution to punching shear resistance but in another, it was insignificant. Therefore, it is necessary to investigate the behavior of flat plates subjected to concentric vertical loading and examine if the ECC is valid as a retrofitting technique through numerical simulations considering various design parameters.

This thesis evaluates the impact of the ECC strengthening technique on the punching shear response of flat plate structures. For that purpose, analytical models of the interior slab-column assemblage were developed in finite element software ABAQUS. First, the model was calibrated from test results in the literature. The numerical simulations were carried out on flat plate models subjected to gravity loading to investigate the global response of the flat plate and its failure mechanism. The contributions of concrete and ECC were determined to examine the effectiveness of ECC strengthening. Moreover, the cracking pattern was visualized by presenting the contour plots that displayed the flat plate model’s maximum principal equivalent plastic strain. In this thesis, the main study parameter was the placement of the retrofitting: on the tension, compression, and both slab surfaces. The other study parameters include compressive strength, thickness, and width of the ECC.

The numerical study results showed that the punching shear behavior of flat plates was improved with the application of the ECC retrofitting technique. The addition of a thin layer of ECC on the compression side of the slab provided a direct shear strength contribution near the column face, therefore no improvement was observed as the width of the ECC increased.

Moreover, the deformation capacity of the slab improved with low-strength ECC retrofitting of the slab on the compression side, whereas normal-strength ECC showed a more brittle response. The addition of a thin layer of ECC on the tension side of the slab has no direct shear force resistance contribution. However, it can lower the neutral axis and enlarge the concrete compression zone, increasing the concrete contribution to the punching shear strength. This increase is only effective if the ECC width is large enough to cover the punching cracking region. The double-sided retrofitting can significantly increase the strength and deformation capacity of the flat plate, resulting in a better performance under punching load. However, it must be noted that the strength does not result from the superposition of strengths of one-sided retrofitting since peak strengths occur at different displacements for ECC retrofitting on the tension and compression sides. Overall, the parametric results revealed that the higher the compressive strength and thickness of the ECC, the greater the punching shear response of the slab. Accordingly, the compressive strength of 20 MPa, thickness of 30 mm, and width of full slab length applied on both sides of the slab were determined to be optimal parameters for improving both strength and deformation capacity.

Acknowledgments

First, I express my sincere gratitude and acknowledge to my supervisor Dr. Dichuan Zhang for his unwavering support, guidance, constructive feedback, and valuable advice during my study period.

I also would like to thank Dr. Jong Kim for his constant encouragement and support throughout my graduate studies.

I wish to extend my gratitude to my dear colleagues and friends for their support and assistance.

Most importantly, I am incredibly grateful to my family for their unwavering love, endless encouragement, and constant inspiration.

Table of Contents

List of Notations

A_s	Area of slab reinforcement
A_v	Area of shear reinforcement
b_0	Critical shear perimeter
b_p	Critical section perimeter
d	The effective depth of the slab
E_0	Initial elastic modulus
E_{sec}	Secant elastic modulus
F_{ct}	Vertical component of tensile force of concrete
F_{dow}	Dowel action
f_c	Compressive strength of concrete
f_{ck}	Characteristic strength of concrete
f_{cm}	Mean compressive strength of concrete
f_{ct}	Tensile strength of concrete
f_s	Yield strength of reinforcing bar
G_f	Concrete fracture energy
G_{f0}	Base concrete fracture energy
K	The coefficient for the deviatoric cross-section
k	Size effect
n_c	Stress concentration factor
r_0	Column diameter
r_1 and r_2	Punching crack radii
s	Spacing of shear reinforcement
s_{eff}	Effective spacing of the reinforcement
$V_{Rd,c}$	Design value of the punching shear resistance
V_a	Aggregate interlock contribution
V_c	Vertical component of shear provided by concrete
V_d	Dowel action
V_n	Nominal shear resistance
V_s	Shear resistance by steel
V_u	Factored shear force
X	Compression zone depth

x	Height of the compression zone
ε_c	Strain at maximum stress
ε_u	Ultimate strain
σ_s	Axial tensile stress
φ_s	Rebar diameter
ε	Eccentricity
ψ	Dilation angle
v	Poisson's ratio
w	Crack width
α	Punching crack angle
β	The ratio of column long side relative to short side length
θ	Tilted crack angle
λ	Factor for lightweight-aggregate concrete
μ	Viscosity
μ and η	Size effect
ρ	Reinforcement ratio
φ	Shear strength reduction factor

List of Figures

List of Tables

Chapter 1 – Introduction

1.1. Overview

A flat plate structural system is one of the most regularly employed flooring systems in reinforced concrete structures due to its numerous benefits such as simplicity in construction and flexibility in terms of design. As slabs are directly supported by columns rather than beams, it provides benefits such as simplified formwork and reduced construction time and cost. On the other hand, slab-column systems are at risk of punching shear failure, a fragile failure that occurs suddenly. The punching shear failure happens because of the extreme concentration of bending flexure and shear force transfer in the slab-column connections. Moreover, additional unbalanced moments developed through eccentric loading or lateral loading increase the possibility of failure and could eventually cause the entire structure to collapse. One of the worst punching shear disasters recorded in history – over 500 people died when the five-story Sampoong Department Store collapsed in South Korea in 1995 [1]. The major reason for the failure was excessive loading and poor design. Furthermore, Bullock's Department Store collapsed by punching shear failure mode in 1994 due to the Northridge earthquake [2]. Thus, it is critical to understand the punching shear mechanism and improve its shear resistance.

There are various strengthening techniques developed over the years to improve the flat plate's capacity to withstand punching shear including the use of column capitals, shear reinforcement, and drop panels [3-5]. Several such methods have been studied and provided the deformation capacity, ductility, and durability of the slab-column joints; however, they are complicated, challenging to install, and aesthetically unappealing. Thus, in this study, to avoid the use of drop panels and shear reinforcement and considering the pseudo-strain-hardening behavior, strengthening of the slab by adding a thin layer of the engineered cementitious composites (ECC) on the slab surface is investigated.

The literature research reveals that most research done to date has used experiments to look into the effects of ECC on the connection between the slab and column. Previous experimental studies focused on limited design parameters due to economic constraints. The ECC might improve the strength capacity of the flat plate structures according to the test results [6, 7]. However, some contradictory findings were obtained from different tests. For example, the contribution of the ECC applied on the tension side of the slab to the punching shear strength was little in one test [6] but noticeable in another one [7]. Therefore, this thesis explores different design parameters for the flat plate structure strengthened with the ECC using numerical simulations. Furthermore, the previous studies did not consider the ECC strength,

width, and thickness as parameters. Thus, this thesis will incorporate the impact of all these parameters on punching shear strength.

The study aims to examine the influence of ECC retrofit on punching shear performance for a flat plate system. This study focuses on numerical methods for the investigation of punching shear behavior under monotonic loading. For that purpose, the analytical model of the interior slab-column joint was developed in finite-element method software, ABAQUS. First, the experimental data from the literature was used to validate the model. The calibrated model was then employed to perform an analytical study to better understand the punching shear performance of flat plates with and without ECC retrofitting under punching loading. Further, the parametric study was executed to identify the optimum parameters of ECC for strengthening the flat plate structures.

1.2. Research hypothesis

The research hypothesis of this study is:

- The use of ECC retrofitting will improve the punching shear behavior of the flat plate.
- A detailed parametric study will reveal the effective ECC parameters that enhance the punching shear performance.

1.3. Research objectives

The thesis aims to evaluate the impact of ECC retrofitting on the punching shear response of flat plate structures. The following are the main objectives of this study:

1. Development of an analytical model of flat plate retrofitted with ECC.

A calibrated three-dimensional finite element model of the interior slab-column assemblage placed upside down is developed for static analysis under punching load. For that purpose, the prototype flat plate structure is designed according to local design code provisions.

2. Evaluation of the performance of ECC retrofitted flat plate under punching load.

A downward vertical displacement is applied on top of the column to imitate the punching load. The load versus displacement curves were plotted to study the effect of ECC retrofitting.

3. Examination of the contribution of concrete and ECC on the punching shear strength of the flat plate.

The contributions of concrete and ECC were determined to determine the impact of each component on the global punching shear response of the flat plate.

4. Investigation of the impact of design parameters of ECC that affect the punching shear behavior of flat plates.

The parametric study results were used to determine the optimum ECC parameters that show better punching shear performance.

1.5. Thesis Structure

There are five chapters in this thesis. The first chapter presents the background on flat plates, the problem statement, and the scope of the work.

The second chapter presents detailed background information about related topics. First, the punching shear mechanism is explained by reviewing the existing mechanical models. Then, the design equations in code provisions are discussed. Furthermore, the chapter contains a literature review on existing retrofitting techniques of flat plates. Finally, the application of ECC retrofitting on a flat plate is discussed.

The third chapter describes the analytical model. This chapter contains the design of the prototype building, a description of the model element, material properties, and the calibration of the model.

The fourth chapter provides the numerical results including the global response, contribution of concrete and ECC, and cracking patterns. Moreover, the parametric study results including the effect of ECC compressive strength, thickness, width, and location can be found in this chapter.

The fifth chapter contains the conclusions, limitations, and future work.

Chapter 2 – Literature Review

2.1. Punching shear mechanism

Punching is an extremely complex failure mode that has been the topic of several studies and attempts at explanation for decades. The connection of slab and column is typically the most crucial part of the flat plate structure in terms of strength because of the significant shear force concentration in this area. In a flat plate structural system, the slab-column assemblage is susceptible to both bending and shear force. The first sign of bending damage is the flexural crack initiation on the slab's tension surface, which is then followed by steel bar yielding. Furthermore, the shear stresses in slabs result in the occurrence of inclined shear cracks. As stresses increase, inclined cracks propagate toward the tension and compression zones, eventually leading to failure. Figure 2 illustrates the failure of the slab-column joint caused by the punching load. The mechanism of punching shear collapse has been the subject of numerous experimental and numerical research published since the 1950s. Thus, several mechanical models have been created that influenced the design code regulations or explored the new aspects of the slab's behavior during shear.

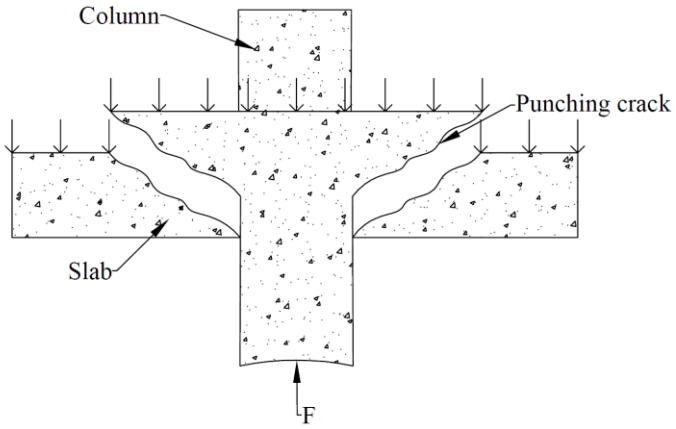

Figure 2.1. Punching shear failure mechanism.

2.1.1. Model proposed by Shehata

In 1989, Shehata and Regan [8] suggested a punching shear failure model based on experimental and numerical analyses of slabs resting on circular columns. According to the typical crack pattern observations, the slab was splatted into rigid radial sections rotating around the neutral axis level center of rotation, which is illustrated in Figure 3. However, the initially proposed model was too complicated to be employed by the designers or to be implemented in design codes. Thus, in 1990, Shehata [9] simplified his model.

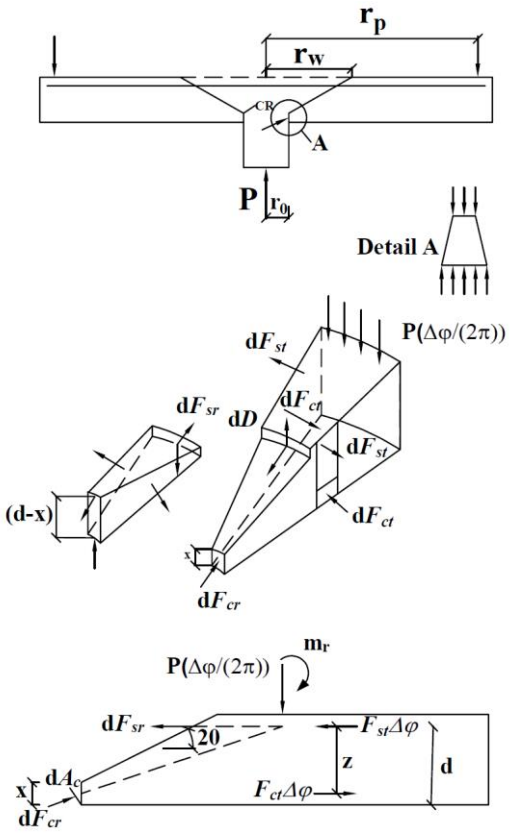

Figure 2.2. Punching shear model reproduced from Shehata and Regan [9].

The following are the forces that contribute to punching shear resistance and were involved in the analysis of each segment:

- Applied load, $P\left(\frac{\Delta\varphi}{2\pi}\right)$;
- The components of tensile and compressive forces: $F_{st}\Delta\varphi$ and $F_{ct}\Delta\varphi$;
- The inclined force of bearing of concrete, dF_{cr} at the column face;
- The steel's radial net forces, dF_{sr}.

Consequently, the punching shear resistance of the flat plate is calculated by

$$P = 2\pi r_0 x n_c f_c tan10^{0\,3}\sqrt{\frac{500}{d}} \qquad (2.1)$$

where r_0 is the column diameter, $n_c = 1.4(\frac{2d}{r_0})^{\frac{1}{2}}$ is the stress concentration factor, and $x \approx 0.8d(np)^{1/2}$ is the compression zone height.

2.1.2. Model proposed by Menetrey

Menetrey [10] established a model to determine the punching shear strength through experimental and numerical studies in 1996. The basis of the suggested model is that the

punching shear strength of concrete is impacted by tensile stress of concrete. The punching force is therefore estimated through the combined effect of the tensile stress's vertical components and the dowel forces of rebars. Consequently, the punching load is expressed as

$$F_{pun} = F_{ct} + F_{dow} + F_{sw} + F_p \tag{2.2}$$

where F_{ct} is concrete's tensile strength, F_{dow} is the dowel action, F_{sw} is the shear reinforcement contribution, and F_p is the force attributed to the prestressed tendon strength. The contribution of concrete's tensile strength, F_{ct}, is derived from the nonlinear finite element evaluation and determined by the following parameters: the reinforcement ratio (ρ), the tensile strength of concrete (f_{ct}), size effect (μ and η), and punching crack radii (r_1 and r_2):

$$F_{ct} = \pi(r_1 + r_2)sf_{ct}^{2/3}\xi\eta\mu \tag{2.3}$$

The dowel force is given by

$$F_{dow} = \frac{1}{2}\sum \varphi_s^2\sqrt{f_c f_s(1-\xi^2)}\, sin\alpha \tag{2.4}$$

where φ_s is the rebar diameter, f_s is the yield strength of the reinforcing bar, f_c is the compressive strength of concrete, and α is the reinforcement and punching crack angle. The term $(1-\xi^2)$ is an expression that describes the parabolic interaction of the axial and dowel force, where $\xi = \sigma_s/f_s$, σ_s is the axial tensile stress.

The shear reinforcement contribution depends on the yield strength of the rebar and is given by

$$F_{sw} = \sum A_{sw}f_{sw}\sin(\beta_{sw}) \tag{2.5}$$

where β_{sw} is the stirrup angle of inclination.

The prestressed tendon force is given as

$$F_p = \sum A_p\sigma_p\sin(\beta_p) \tag{2.6}$$

where A_p is the prestressing tendon area, σ_p is steel's tensile stress, and β_p is the angle of inclination of the tendon.

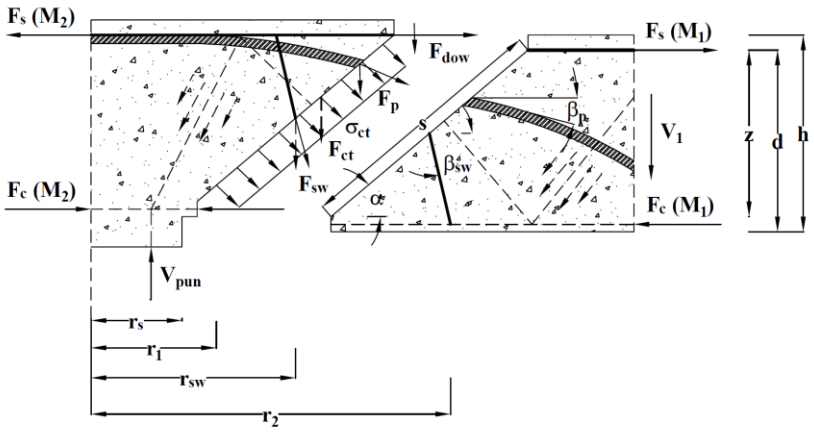

Figure 2.3. Punching shear model reproduced from Menetrey [10].

2.1.3. Model proposed by Theodorakopoulos and Swamy

Theodorakopoulos and Swamy [11] investigated that the slab-column connection undergoes several stages of deformation under increasing load in 2002. At the initial stage, on the slab's tension surface, roughly circular fractures initiate along the column perimeter and develop towards the compression zone. Then, new flexural cracks in lateral and diagonal directions are created. At 50-70% of the peak load, the tilted fractures appear around the middle of the depth of the slab. As the application of an increasing load, the inclined cracks propagate to the compression side and tension steel. Eventually, the failure occurs at the compression zone by punching shear mode. The total shear resistance is determined by

$$V_u = V_c + V_a + V_d \tag{2.7}$$

where V_c is the vertical portion of the concrete's resistance to shear at the compression side, V_a is the aggregate interlock contribution and V_d is the dowel action. However, the impact of aggregate interlock can be disregarded at the failure stage due to the considerable distance between crack faces. The yielding stress of the steel rebar and the tensile strength of concrete are the primary forces behind the dowel action. Thus, the equation for the ultimate punching strength is given by

$$V_u = b_p X cot\theta f_{ct} \tag{2.8}$$

where b_p is the critical section perimeter, f_{ct} is the tensile strength of concrete, X is the compression zone depth, and θ is the tilted crack angle.

2.1.4. Model proposed by Alexander and Simmonds

A truss theory for modeling the behavior of a flat slab subjected to both gravity and unbalanced moments was suggested by Alexander and Simmonds [12]. There were several

assumptions made to develop the truss analogy. The truss model consisted of inclined concrete compression struts and horizontal tensile steel ties. There were two varieties of compression struts that were taken into consideration: 1) shear struts that were inclined to an angle α and 2) anchoring struts that were parallel to the slab plane. The anchoring struts were in-plane with reinforcement bars. Specifically, uplift struts opposed the upward action and were connected by bottom mat steel, whereas gravity struts were the shear struts that opposed the slab's downward movement and were joined by the top mat steel. The assembly of the load-resisting struts is illustrated in Figure 2.4. With increasing the ratio of the moment to shear, the anchoring struts replaced the gravity struts. Based on the analysis, the maximum capacity of the truss model depends on the yielding of steel ties. Eventually, Alexander and Simmonds derived the following equations:

$$tan\alpha = 1 - e^{-0.85K} \tag{2.9}$$

where

$$K = \frac{s_{eff} d\prime \sqrt{f\prime_c}}{A_{bar} f_y (c/d_s)^{0.25}} \tag{2.10}$$

The term $tan\alpha$ was referred to as the out-of-plane shear load divided by the in-plane shear force of the compression strut. In equation 12, s_{eff} is the effective reinforcement spacing, f'_c is the compressive strength of concrete, d' is the concrete cover, A_{bar} is the reinforcement area, and f_y is the yield strength of rebar. The parameter c/d_s was employed to decrease the shear strength as the rectangularity of the column increases, where d_s is slab's effective depth and c is the width of the column. The value of 0.25 was derived from trial-error analysis.

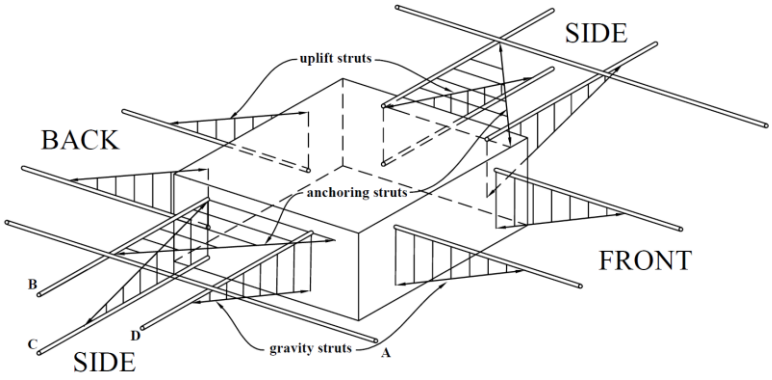

Figure 2.4. The proposed truss model reproduced from Alexander and Simmonds[12].

According to the authors, there are only two possible failures based on the truss model including the concrete failure at the compression zone before steel yielding or steel yields and α value reaches some limit.

2.2. Punching shear in design codes

The punching shear failure in flat plate structures most frequently occurs at the place of the slab closest to the column face. A flat plate may experience an unbalanced moment and excessive shear force as a result of lateral deformation that occurs during an earthquake.

2.2.1. ACI-318 code provisions

According to the ACI Code provisions [13], the factored shear force, V_u, due to the applied loads should be larger than the nominal shear resistance, V_n. The basic equation for shear design is

$$\varphi V_u \geq V_n \tag{2.11}$$

where the factor of strength reduction for shear, φ, is 0.75. The shear resistances attributed to the concrete, V_c, and shear reinforcement, V_s. add up to the nominal shear resistance.

$$V_n = V_c + V_s \tag{2.12}$$

The impact of concrete on the nominal shear resistance is determined by the least value obtained from the following equations:

$$V_c = 0.33\lambda\sqrt{f'_c}b_0 d \tag{2.13}$$

$$V_c = \frac{1}{12}\left(2 + \frac{4}{\beta}\right)\lambda\sqrt{f'_c}b_0 d \tag{2.14}$$

$$V_c = \frac{1}{12}\left(\frac{\alpha_s d}{b_0} + 2\right)\lambda\sqrt{f'_c}b_0 d \tag{2.15}$$

where λ is the factor for lightweight aggregate concrete, f'_c is the concrete's compressive strength, b_0 is the critical shear perimeter, β is the long side divided by the short side of column dimensions, and α_s is equivalent to 20 for the corner, 30 for the edge, and 40 for interior columns. The critical shear section perimeter is measured at a d/2 distance from the slab-column joint.

The shear reinforcement contribution is defined by

$$V_s = A_v f_{yt}\frac{d}{s} \tag{2.16}$$

where A_v is the shear reinforcement area, f_{yt} is the yield strength, d is the slab's effective depth, and s is the spacing.

The consistent transmission of shear stresses over the critical perimeter close to the column affects the punching shear forces at the joints of the slab and column. Additionally, the

influence of lateral stress causes unbalanced moments to be generated. When the lateral loads or unbalanced moment is applied, the maximum shear stress is calculated by

$$v_u = \frac{V_u}{b_0 d} \pm \frac{\gamma_v M_u c}{J_c} \quad (2.17)$$

where V_u is the factored shear force, M_u is the factored imbalanced moment, c is the eccentricity, J_c is the polar moment of inertia, and γ_v is the unbalanced moment fraction transmitted by shear stresses at slab's critical perimeter.

The parameter γ_v is defined as

$$\gamma_v = 1 - y_f \quad (2.18)$$

The parameter y_f is the component of the unbalanced moment transmitted by flexure and is determined by

$$\gamma_f = \frac{1}{1+\frac{2}{3}\sqrt{b_1/b_2}} \quad (2.19)$$

where b_1 and b_2 are the critical section widths parallel to and perpendicular to the axis.

The polar moment of inertia, J_c, is determined by

$$J_c = \left(I_x + I_y\right) + A\bar{x}^2 \quad (2.20)$$

where $\bar{x}$ is the distance from the critical perimeter centroid and I_x and I_y are moments of inertia.

2.2.2. Eurocode 2 provisions

According to the Eurocode 2 [14], the critical shear region is taken as 2d distance from the slab-column joint. The punching shear resistance is determined by the following equation

$$V_{Rd,c} = C_{Rd,c} k (100 \rho f_{ck})^{1/3} \geq v_{min} \quad (2.21)$$

where

$$C_{Rd,c} = \frac{0.18}{\gamma_c} = \frac{0.18}{1.5} = 0.12 \quad (2.22)$$

k is the size effect and is given by

$$k = 1 + \sqrt{\frac{200}{d}} \leq 2.0 \quad (2.23)$$

ρ is the reinforcement ratio and is given by

$$\rho = \sqrt{\rho_y \rho_z} \leq 0.02 \quad (2.24)$$

$$v_{min} = 0.035k^{\frac{3}{2}}f_{ck}^{\frac{1}{2}} \quad (2.25)$$

and f_{ck} is the cylinder compressive strength of concrete.

The factored shear resistance is determined by

$$v_{Ed} = \frac{\beta V_{Ed}}{u_0 d} \leq v_{Rd,max} \quad (2.26)$$

where β coefficient corresponds to the unbalanced moment transfer and is given by

$$\beta = 1 + 1.8\sqrt{\left(\frac{e_y}{b_z}\right)^2 + \left(\frac{e_z}{b_y}\right)^2} \quad (2.27)$$

where e_y is eccentricity along y-axis and e_z is eccentricity along z axis, b_y and b_y are widths of the critical section.

However, due to its poor seismic performance, flat plate structures are prohibited in high seismic locations under the current seismic design codes. According to ASCE-7 and ACI [15], the flat slab structure may be employed in low seismic areas (SDC A and B) as ordinary moment frames. For moderate seismic zones (SDC C), the flat plate structural system is permitted if it satisfies additional requirements that are related to punching shear capacity, slab reinforcement, and distribution of slab moments. It can therefore be regarded as an intermediate moment frame. The usage of flat slab structures in moderate and high seismic areas is prohibited under Eurocode 8. According to Kazakhstan's seismic design code [16], flat plate structures are permitted in high-intensity locations (intensity 8 and 9, similar to SDC D-E), as well as moderate regions (intensity 7, corresponding to SDC C), with height restrictions of 2 stories, 4 stories, and 5 stories for intensity 9, 8, and 7, respectively.

2.3. Existing retrofitting techniques

Given that the failure caused by punching shear is sudden and catastrophic in nature, it is critical to employ strengthening measures to increase the shear resistance. Extensive research has been done over the past few decades to explore the number of retrofitting techniques. Shear reinforcement, drop panels, and column capitals are only a few of the retrofitting techniques that have been studied over time to strengthen the punching shear response of flat plate systems. Several such methods have been studied and provided the ductility of the connections and deformation capacity.

The utilization of shear reinforcement is one of the common techniques. For example, Robertson et al. [3] have experimentally tested the behavior of flat plate strengthened with three

kinds of shear reinforcement including single-leg stirrups, closed hoop stirrups, and headed-stud shear reinforcement subjected to low gravity and cyclic loadings. Accordingly, it was reported that at 3.5% drift, punching shear failure happened in the control specimens, whereas specimens with shear reinforcement were able to withstand 8% drift without punching shear crack. Overall, the authors have stated that all three forms of stirrups were equivalently successful in preventing punching shear failure at a low gravity shear ratio. Bu and Polak [17] investigated the effect of the shear bolt retrofitting technique on flat plates subjected to both gravity and cyclic loads. It was reported that adding shear bolts raised the drift ratio at maximum load by 66% to 123%. Moreover, it was found that the behavior of the slab is not significantly changed by the shear bolts when they are placed over four times the effective slab thickness. Furthermore, Taresh et al. [18] tested the joint effect of shear bolts and steel angle plates on flat plates' punching shear response. The proposed retrofitting techniques provided a larger punching shear strength and deformation capacity compared to the control specimen. Additionally, the punching shear failure mode was changed to flexure failure, hence reducing the risk of sudden collapse.

Another strengthening technique is utilizing the drop panel as a local thickener. Prawatwong et al. [4] experimentally tested the impact of the use of the drop panel on the seismic behavior of post-tensioned interior slab-column assemblage. It was stated that the drop panel reduced the gravity-to-shear ratio by 54%, from 0.28 to 0.13. According to the results, the control specimen experienced a brittle punching shear failure at around 2% drift, whereas the specimen with a drop panel increased lateral load-bearing capacity by 80% at about 6% drift but also failed by punching shear. However, Megally and Ghali [5] reported that even though drop panels improve the punching shear strength, they have little effect on ductility. Thus, it is not recommended to use drop panels for seismic-resistant slab-column connections.

In addition, a fiber-reinforced polymer (FRP) is another alternative for strengthening the slab-column connections. Over recent years, FRP has become an appealing alternative to conventional retrofitting methods due to its higher tensile strength, corrosion resistance, and lightweight. Sissakis and Sheikh [19] experimentally tested the impact of carbon fiber-reinforced polymer (CFRP) laminates on the shear strength of existing slabs. The results demonstrated a significant improvement in shear strength of about 80% and a substantial increase in ductility of 700%. Furthermore, Kim et al. [20] studied the significant effect of CFRP sheets on enhancing the ultimate load-bearing capacity of flat slabs. Additionally, the cracks were dispersed more uniformly as a result of the CFRP strengthening.

2.4. Engineered Cementitious Composites as a Strengthening Technique

The fundamental characteristic of Engineered Cementitious Composites (ECC) is their pseudo-strain hardening behavior that enables them to endure high tensile loads and thus improve ductility. The ECC consists of cement, fly ash, silica, water, fibers, and viscosity-modifying agents. The micromechanics approach is used to optimize the design of ECC, where the formation of numerous microcrackings delays the fracture localization. As a result, the brittle failure state can be transitioned to a ductile failure mode [21]. Therefore, research studies have been done to investigate the possible application of ECC in punching shear-resistant structures. Experimental research was done by Afefy and Tony [6] to determine how the ultra-high-performance strain-hardening cementitious composite (UHP-SHCC) strengthening approach affected the slab-column joint's punching shear resistance. In the study, the thin layer of UHP-SHCC was applied on the slab's compression as well as the tension side. Although the UHP-SHCC has a better tensile resistance capability, a modest rise of about 8.3% and 3.8% in cracking loads and 5% and 4% in ultimate loads were determined for the slabs, which demonstrates the ineffectiveness of such a technology. The slabs strengthened with UHP-SHCC on the compression side, however, demonstrated the best punching shear resistance, with increases in the initial cracking load of 23%, 18.6%, 38%, and 20.7% respectively. According to the results, of the testing program, it was concluded that the best shear resistance is achieved by cross-strengthening the slab with UHP-SHCC and anchoring it with single-leg stirrups. Furthermore, Amiri and Esfahani [7] studied the ECC impact on punching and post-punching shear strength of flat slabs subjected to imbalanced moments. In this study, ECC strengthening was done on the tension face of the slab with a thickness of 30 mm. A flat plate's punching and post-punching shear capacity are each increased by 16 and 8%, respectively, by the inclusion of a 30 mm ECC retrofit on the tension side. Another research done by Alhussainawe et al. [22] indicates that the incorporation of polyvinyl alcohol fibers engineered cementitious composites (PVA-ECC) and increased slab thickness significantly improves punching shear capacity. Ye and his colleagues [23] investigated how the reinforcement ratio impacts the punching shear strength of slab-column assemblage strengthened with reinforced engineered cementitious composites (RECC). It was stated that the punching shear resistance proportionally enhances with the reinforcement ratio increase. Nevertheless, all these experimental studies considered limited parameters due to the cost issue.

Chapter 3 – Description of the Study

3.1. Design of prototype of flat slab building in Almaty region

In this study, the flat plate connection was designed in the Almaty region using the existing seismic design code of Kazakhstan [13]. The structural member dimensions, reinforcement detailing, and material strength were employed to develop the finite element model. Figure 3.1 and Figure 3.2. demonstrate the plan and elevation view of the prototype structure. Muttoni [24, 25] states that the lines of contra flexure are positioned at a radial distance of roughly 0.2*l*. Similarly, an elastic analysis on SAP2000 indicates that the contra flexure points of the slab are determined to be at 0.2*l* distance far from the slab-column joint, where *l* is the distance from the slab's center to center, which is illustrated in Figure 3.1. Thus, the boundary conditions of an isolated slab model were placed at 0.2*l* distance from the column center. Since the original slab span length was estimated to be 5m, the isolated slab's length at the contraflexure zone is 2.3m. According to the design code of Kazakhstan, SP RK 2017 [16], the smallest allowable slab thickness should be 200mm. Based on SAP2000 analysis, the slab thickness was taken as 250mm. Figure 3.3 illustrates the dimensions of the isolated slab-column model. The top and bottom rebar mesh employed to reinforce the slab is illustrated in Figure 3.4. The flat plate was designed using the EC2 code provisions discussed in Chapter 2.

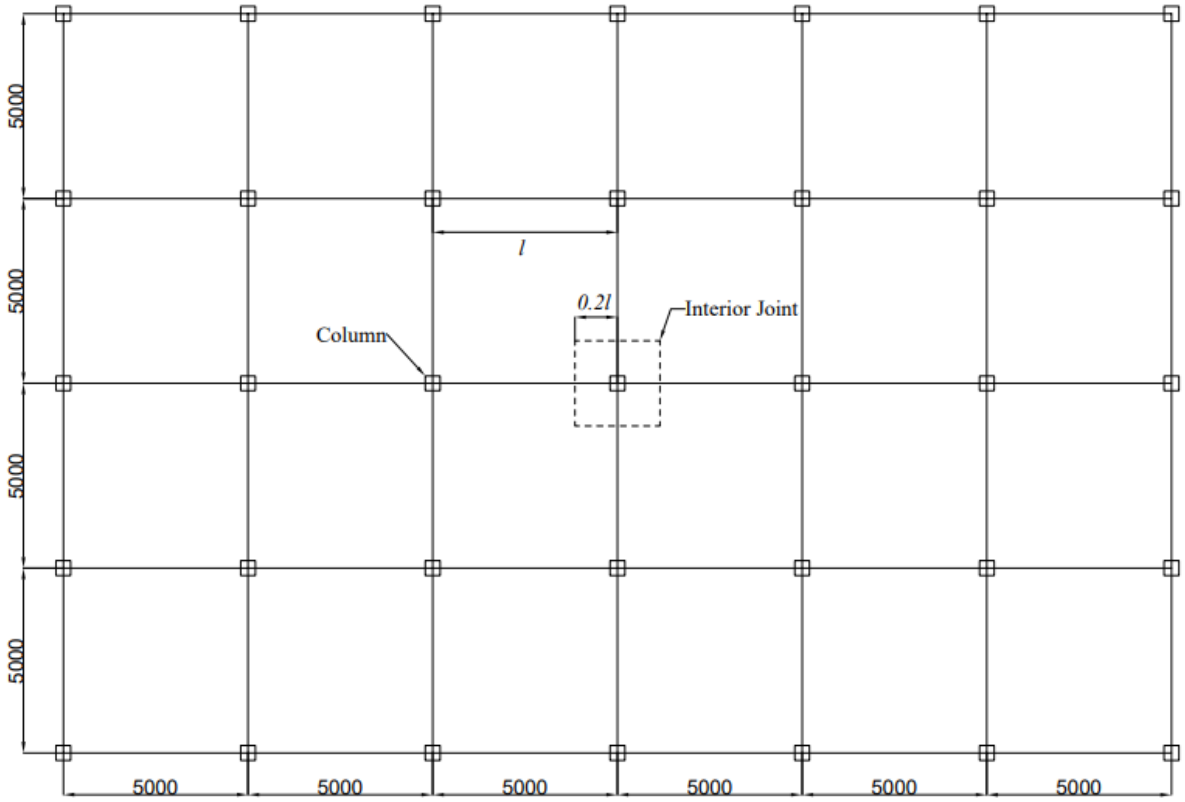

Figure 3.1. Plan view of the prototype building.

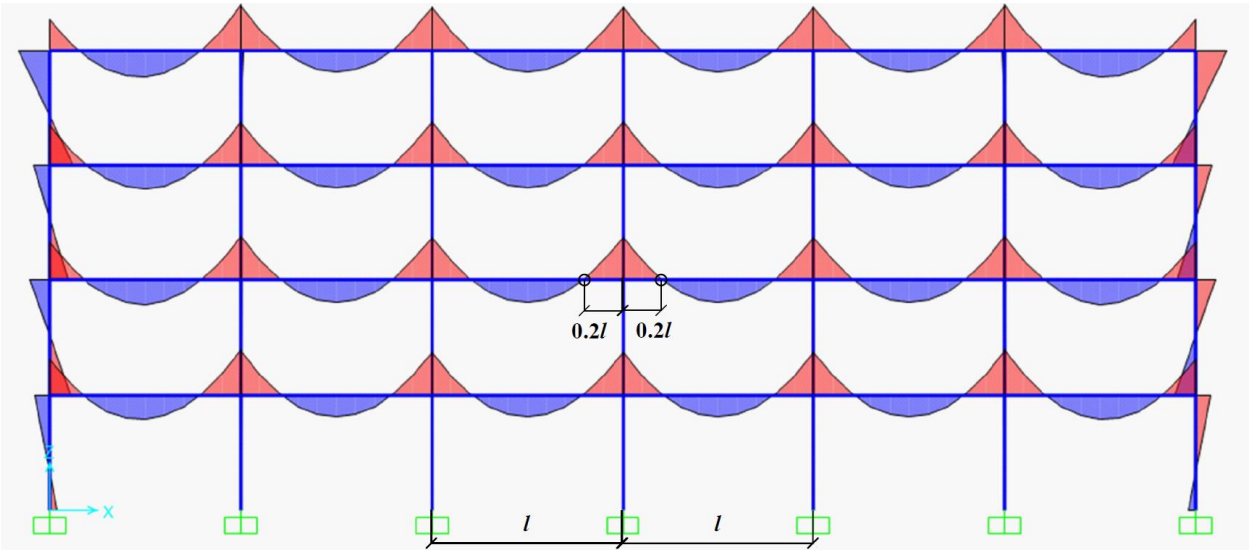

Figure 3.2. Elevation view of the prototype building from SAP2000.

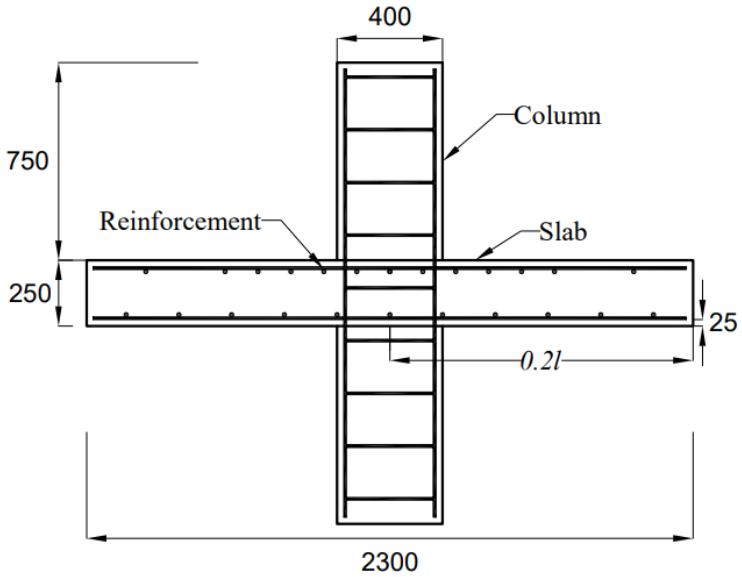

Figure 3.3. Slab-column dimensions.

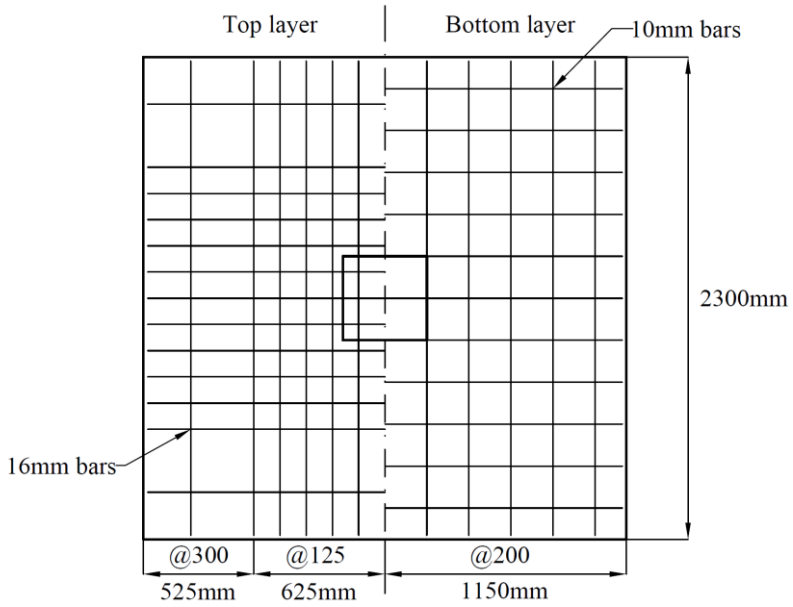

Figure 3.4. Arrangement of reinforcement in slab

3.2. Analytical model

The finite element analysis of the interior flat plate connection was implemented using the software called ABAQUS. The interior slab-column model consists of two types of elements: a) 8-noded hexahedral elements (C3D8R) with decreased integration, which was utilized to model the concrete slab and column, and b) 2-noded linear truss elements (T3D2) that were implemented for reinforcement modeling. The embedded constraints were utilized to create the perfect bond connecting concrete and reinforcement. As for retrofit, the ECC layer was also modeled as an 8-noded hexahedral solid element (C3D8R). The perfect bond between the slab and ECC is achieved by tie constraints. The concrete and ECC were meshed of equal size to make it possible to tie nodes of ECC and slab elements.

In reality, the punching force is applied from the bottom column to the slab. It should be noted that in this study, the model is an upside version of the assemblage with the compression zone at the top and the tension zone at the bottom of the slab as shown in Figure 3.5.

The boundary conditions for the model were introduced at the perimeter of the slab edge as a roller support (Uy=0). The downward vertical displacement with increasing magnitudes was applied at the column's top surface. One-fourth of the specimen was used in the analysis by taking the symmetry of the specimens into account. Therefore, the symmetry boundary conditions were applied on the y-z symmetry plane (Uz=URy=URx=0) and the y-x symmetry plane (Ux=URy=URz=0), where the displacements normal to the plane of symmetry (Uz and

Ux) and rotations around the axis in the plane of symmetry (URx, URy, and URz) are zero. Figure 3.6 illustrates the 3D model of a flat plate developed in the software.

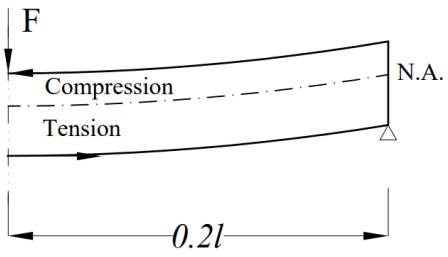

Figure 3.5. Compression and Tension zones in slab

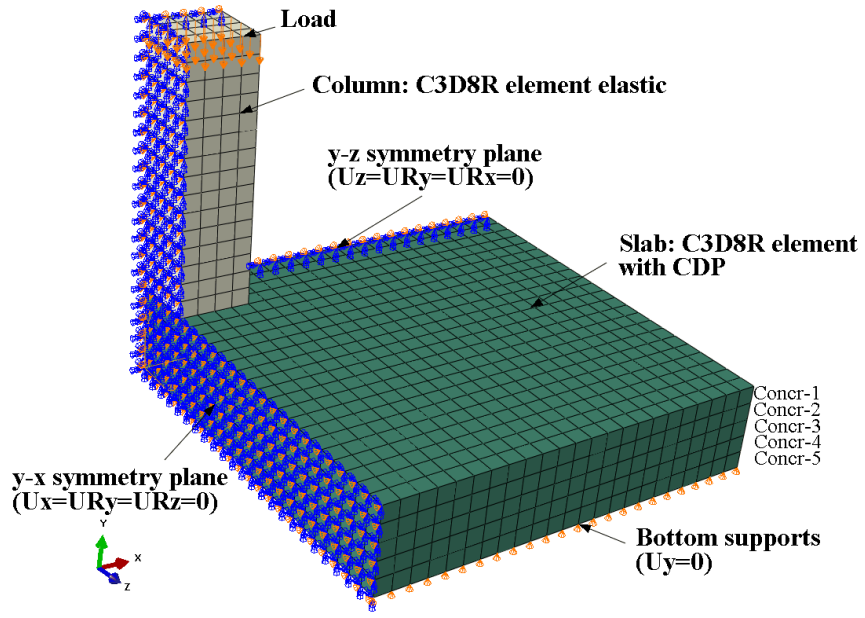

(a)

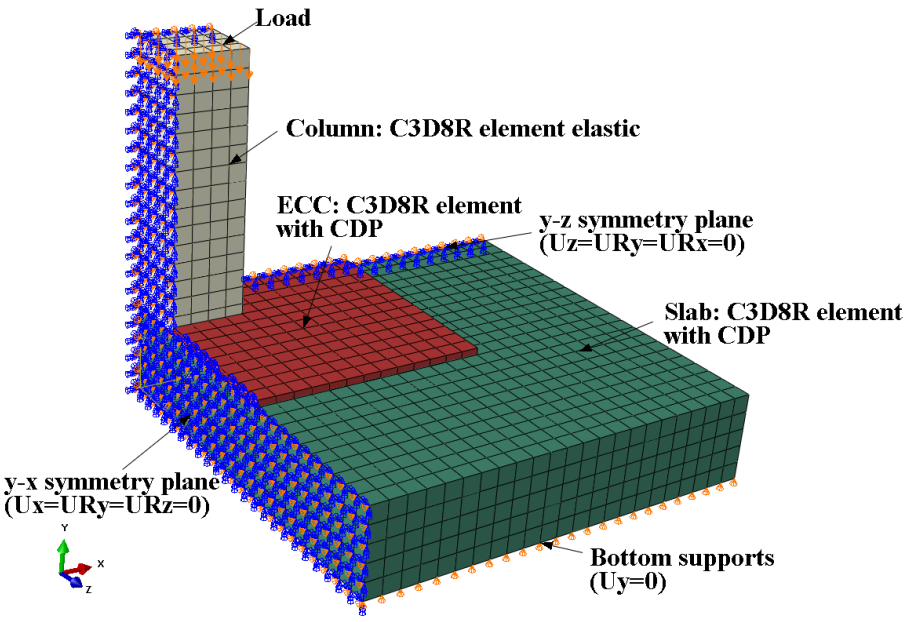

(b)

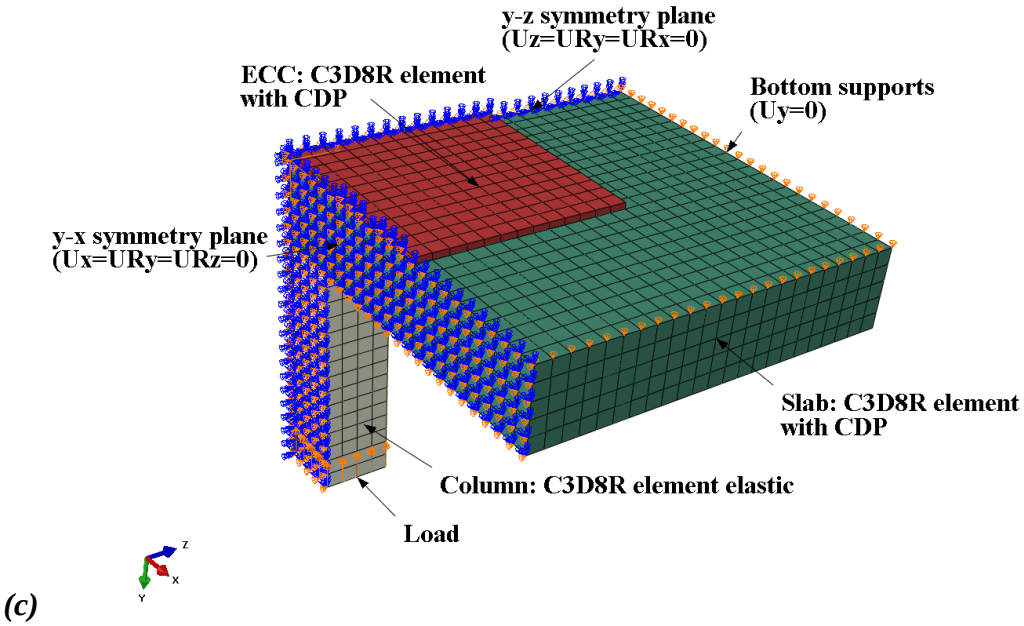

(c)

Figure 3.6. 3D model of a flat plate: (a) unretrofitted, (b) retrofitted on the compression side, and (c) retrofitted on the tension side.

3.3. Material modeling

The concrete material was designed by the concrete damaged plasticity (CDP) model. The CDP model employs the concept of isotropic tension and compression plasticity along with isotropic damaged elasticity to convey the inelastic performance of concrete [26]. The input factors for the elastic region are the elastic modulus (E_0) and Poisson's ratio (v), which was estimated to be 0.15. The modulus of elasticity was calculated by $5000\sqrt{f_c'}$ (MPa). In the inelastic region, input parameters are compressive hardening and tensile stiffening behavior. The compression hardening was simulated using the Hognestad parabola model, in which the three zones can be distinguished in the compression behavior. The first domain is a linear-elastic region that has an initial modulus of elasticity, E_0, and the linear branch is assumed to end at stress 40% of compressive strength. The second region is up to peak load at ε_0, which is determined by $2f'_c/E_{sec}$. The secant modulus of elasticity, E_{sec}, is equal to $5500\sqrt{f_c'}$ (MPa). The third domain is a post-peak response which lasts up to the ultimate strain, ε_u. The compressive stress is determined with the following equation.

$$\sigma_c = f'_c\left[2\left(\frac{\varepsilon_c}{\varepsilon_0}\right) - \left(\frac{\varepsilon_c}{\varepsilon_0}\right)^2\right] \qquad (3.1)$$

The bilinear stiffening response is utilized to develop the concrete tensile behavior, where the tensile response is found from concrete tensile strength, f'_t and concrete fracture

energy, G_f. The tensile strength is estimated to be equivalent to $0.33\sqrt{f_c'}$ (MPa), while concrete fracture energy is calculated by

$$G_f = G_{f0}(f_{cm}/f_{cm0})^{0.7} \quad (3.2)$$

where G_{f0} is the base fracture energy and is estimated to be 0.026 N/mm, f_{cm} is the average compressive strength and determined from $f_{cm} = f_{ck} + 8MPa$, and $f_{cm0} = 10MPa$ [27]. In 1981, Petersson [28] suggested the relationship between tensile stress and crack width, which is presented in Figure 3.7, where G_f is the area under the curve.

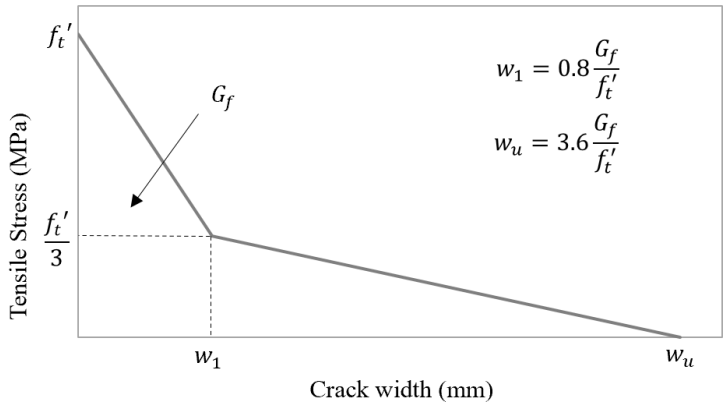

Figure 3.7. Tensile stress-crack width curve for concrete reproduced from Genimkousou [27].

The division of the crack width by element length, which is 50 mm for the following simulations, yields the uniaxial tensile stress-strain relationship. Accordingly, Figure 3.8 demonstrates the uniaxial stress-strain relationship in tension and compression applied to the analytical model. Table 3.1 provides the material properties of concrete.

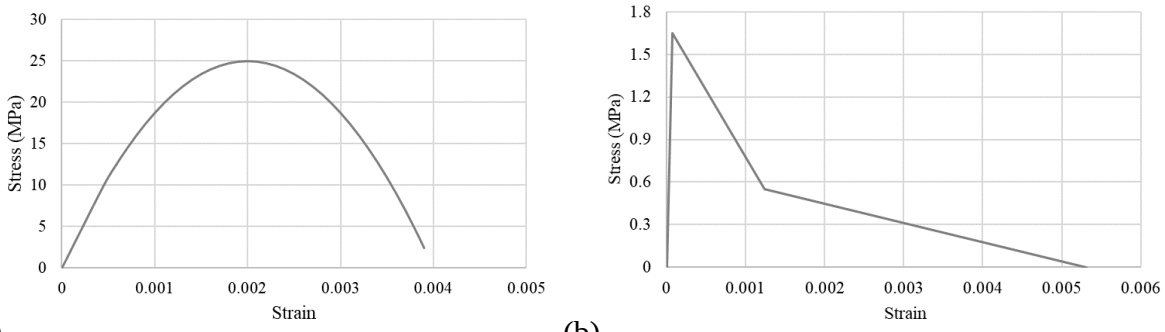

(a) (b)

Figure 3.8. Stress-strain relationship of concrete for CDP model: (a) compression and (b) tension.

Table 3.1. Material properties of concrete.

Compressive strength (MPa)	Tensile strength (MPa)	Elastic modulus (MPa)	Poisson's ratio
25	1.65	27500	0.15

The reinforcement was modeled using the isotropic strain hardening concept for plasticity. The elastic modulus and Poisson's ratio of rebar were estimated to be 200,000 MPa and 0.3, respectively. Table 3.2 provides the mechanical properties of steel from the experimental study of Ozkal (2021) [29].

Table 3.2. Mechanical properties of flexural reinforcement.

Yield strength (MPa)	Tensile strength (MPa)	Maximum strain (%)
427	565	26.51

The input parameters for the plasticity of concrete are given in Table 3.3. The dilation angle and viscosity were iteratively calibrated with the experimental test outcomes which are covered in the following section.

Table 3.3. Input plasticity parameters for CDP of concrete

Parameters	Dilation angle (ψ)	Eccentricity (ε)	f_{b0}/f_{c0}	K	Viscosity (μ)
Values	42^o	0.1	1.16	0.667	0.0001

The ECC was also modeled with a concrete damaged plasticity model. The plasticity parameters for ECC are shown in Table 3.4.

Table 3.4. Input plasticity parameters for CDP of ECC

Parameters	Dilation angle (ψ)	Eccentricity (ε)	f_{b0}/f_{c0}	K	Viscosity (μ)
Values	30^o	0.1	1.16	0.667	0.001

The compressive and tensile behavior of ECC follows the stress-strain relationship illustrated in Figure 3.9. The compressive stress-strain relationship of ECC initially follows the linear elastic curve until 40% of its peak compressive strength. In the following domain, the stress-strain relationship is inelastic and nonlinear up to the peak compressive strength of ECC, σ_c. Then, the stress descends to residual strength, which is 40% of its peak strength. The

ultimate strength of ECC is assumed to be 15% of its peak strength. The tensile stress-strain relationship of ECC represents the strain-hardening behavior of ECC. According to the stress-strain curve, the tensile behavior of ECC can be divided into three domains that are the linear-elastic region, strain hardening, and strain softening. The first cracking strength is defined as σ_{t0}, then it keeps increasing until its peak tensile strength, σ_{tp}. Finally, the ultimate strength of ECC is assumed to be 5% of its cracking tensile strength.

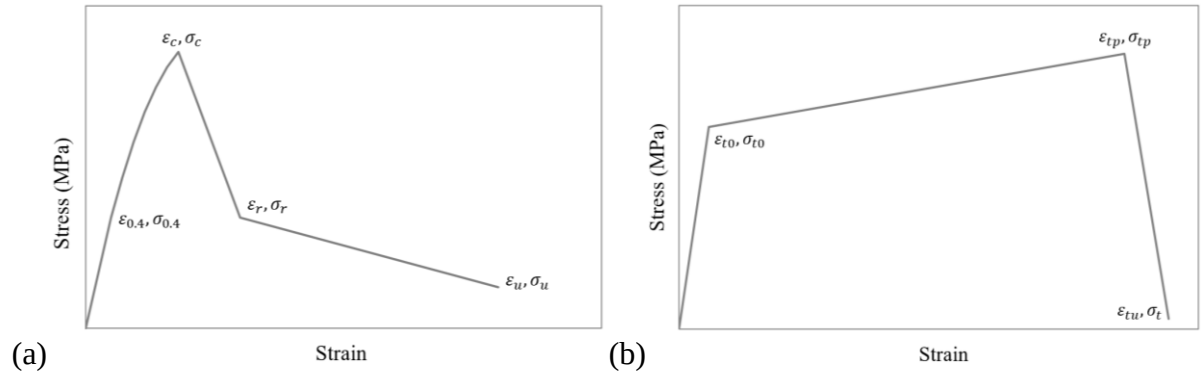

Figure 3.9. a) compressive and b) tensile stress-strain relationship of ECC [30].

The mechanical properties of ECC were determined from the literature review on experimental testing research. Table 3.5 provides the parameters of ECC required to build compressive and tensile stress-strain curves shown in Figure 3.9.

Table 3.5. Mechanical properties of ECC

Compressive strength (MPa)	Density (kg/m^3)	Young's modulus (GPa)	First tensile cracking strength (MPa)	Peak tensile strength (MPa)
10	903	2.87	1.37	2.03
20	1128	6.28	1.93	2.71
30	1354	9.69	2.50	3.40
40	1580	13.10	3.07	4.09
50	1806	16.51	4.20	5.46

3.4. Model calibration

The analytical model was first verified from the existing experimental outcomes in the literature. For that purpose, the experimental testing conducted by Afefy and El-tony [6] was used. Two specimens of the interior slab-column assemblage with and without the ECC layer were used to calibrate the model. The overall dimensions of the slab were 1000 mm x 1000 mm x 120 mm. The flat plate dimensions and reinforcement details are given in Figure 3.10. The

concrete compressive strength was 30 MPa cubic strength and all specimens were reinforced with 10 mm bars with yield strength of 420 MPa. The ultra-high-performance strain-hardening cementitious composite (UHP-SHCC) material is employed as a retrofitting technique. The thickness of the UHP-SHCC material was 20 mm and was applied in the compression and tension side of the slab. The compressive and tensile strengths of UHP-SHCC were 54 MPa and 5.50 MPa, respectively. The specimens were subjected to displacement-controlled loading until failure.

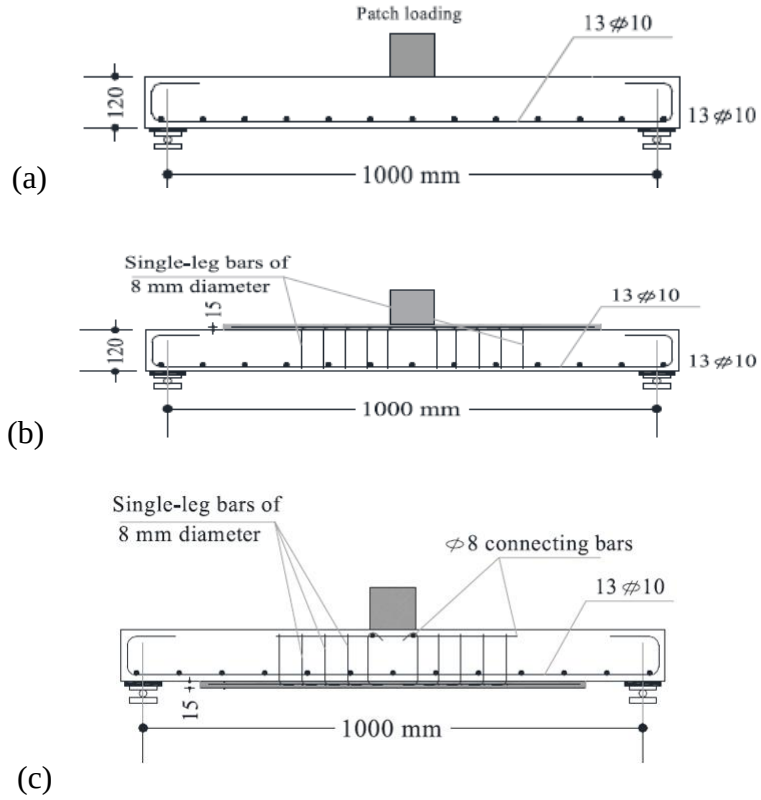

Figure 3.10. Dimensions and reinforcement detailing of the experimental setup: a) without ECC; b) with ECC on the compression side; c) with ECC on the tension side [6].

Figure 3.11 demonstrates the global response comparison of the numerical analysis and outcomes of the experiment. As can be observed, the analytical model provides a similar behavior with experimental test results achieving similar strength, but somewhat higher stiffness. The discrepancy in stiffness might happen since FEM analysis does not consider laboratory conditions where cracking might occur due to shrinkage, transportation, and temperature. Furthermore, the bond between concrete and reinforcement is assumed to be a perfect bond by using the embedded constraints, which overestimates the stiffness of the connection compared to the experimental testing results. In order to quantify the simulation variations, the least square method was used by comparing simulation and experimental results. The obtained coefficient of determination (R^2) is given in Figure 3.11. The coefficient of

determination ranges from 0.63 to 0.94, which indicates a good correlation between experimental and numerical test results. Overall, the results of the simulation are compatible with experimental test outcomes, therefore, these calibrated model parameters can be utilized for further study.

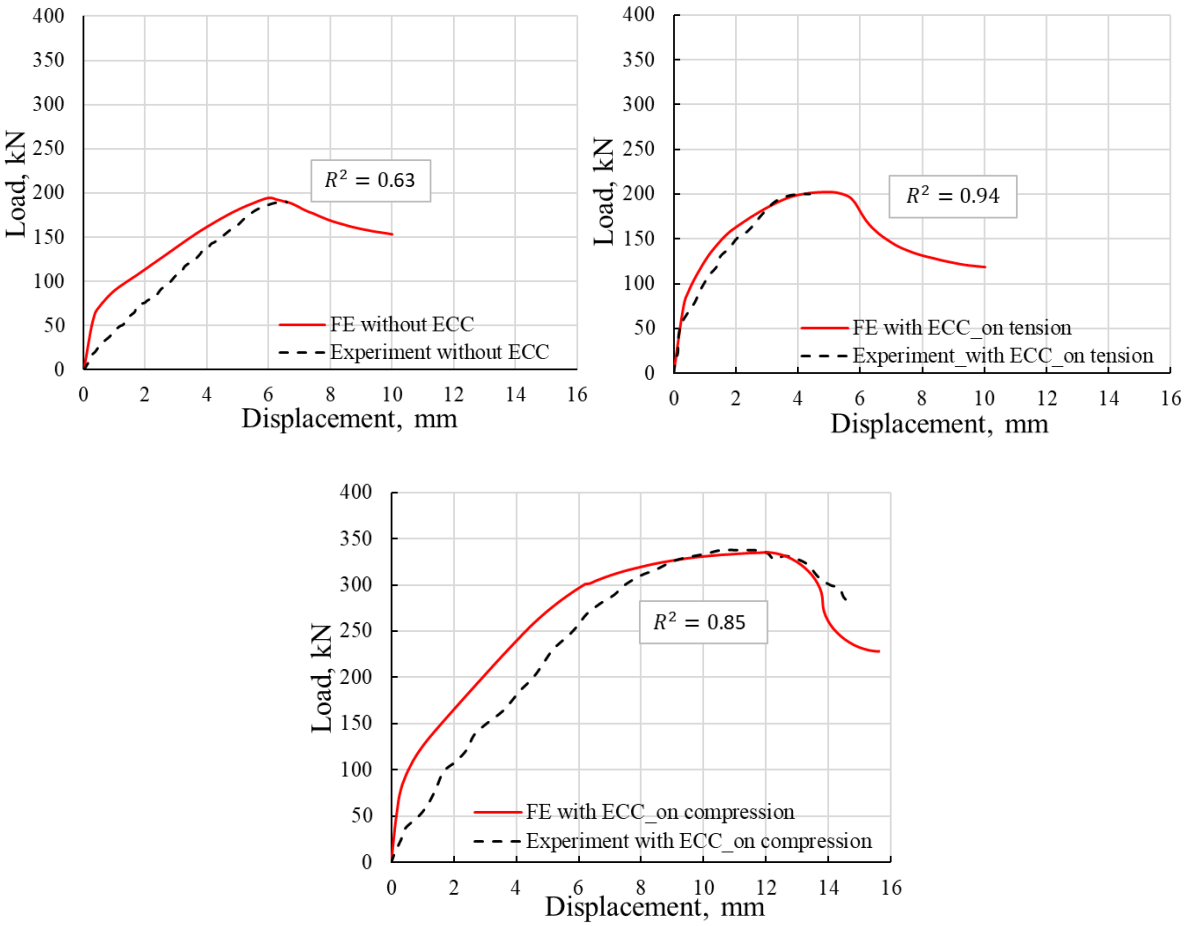

Figure 3.11. The comparison of load-displacement behavior with experimental results.

3.5. Study Parameters

The parametric study was conducted to determine the impact of ECC retrofit on the improvement of punching shear performance of slab-column joints. A total of four parameters were studied. The main parameter is the location of the ECC layer on the slab. There were two contradictory studies regarding the performance of tension-side retrofitting [6, 7]. Therefore, it is important to determine whether the tension side strengthening is valid in flat plates. Furthermore, in this study, the effect of the ECC layer applied on compression and both sides is investigated.

One of the most crucial parameters is ECC compressive strength. The low-strength ECC offers some benefits such as low weight and thermal insulation, despite its lower mechanical

properties. In this study, the compressive strength of low-strength ECC was between 10 and 20 MPa. In addition, the parametric study includes the normal strength ECC of 30 to 50 MPa compressive strength.

Another important parameter considered in the parametric study is the ECC layer width. A failure caused by punching shear usually happens at the region of the critical perimeter of the slab. According to EC2, the critical perimeter is taken 2d distance from the slab-column joint, where d is the slab's effective depth. Thus, in the parametric study, the ECC retrofit widths were taken to be less, equal, and more than the critical perimeter, which is 1d, 2d, 3d, and full slab length distance from the column.

The parametric study includes the thickness of ECC retrofit. Since ECC is more expensive than conventional concrete, it is significant to determine the proper thickness of ECC. Therefore, ECC thicknesses of 15mm, 20mm, 25mm, and 30mm were tested. The study parameters are summarized in Table 3.6. In total, 240 runs were conducted with different combinations of study parameters.

Table 3.6. Parametric study

#	Varying parameters	Values used	# of runs
1	ECC Compressive strength	10, 20, 30, 40, 50 MPa	5
2	ECC thickness	15, 20, 25, 30 mm	4
3	ECC width	1d, 2d, 3d, full	4
4	ECC location	Compression, tension, and both	3
		Total	**240**

Chapter 4 – Numerical Results

In this chapter, the results of monotonic loading analysis on flat plates and parametric study are provided. The impact of ECC on punching shear resistance is investigated in terms of study parameters including compressive strength, thickness, width, and retrofitting sides of ECC and their effect on global response, local response, and cracking pattern.

4.1. Compression side retrofitting

4.1.1. Global response

The global load versus displacement response of a flat plate with varying ECC compressive strengths from 10 MPa to 50 MPa and width from 1d to full is presented in Figure 4.1. Firstly, it is obviously seen that the slab-column assemblage with ECC retrofitting has greater strength than the unretrofitted flat plate. The addition of the thin ECC layer on the compression surface of the slab considerably enhances both strength and deformation capacity and remains constant despite of width increase. Since the punching shear crack propagates towards the compression zone and the failure happens at the joint of slab-column, retrofitting is only effective at the place of the joint. Furthermore, the low-strength ECC provides a higher deformation capacity for flat plates. However, when the strength is greater than 20 MPa, the deformation capacity starts to decrease. This demonstrates that adding low-strength ECC can improve strength and ability to withstand deformation. This might be because ECC generally shows ductile behavior under compression, thus, at a higher strength it tends to be more brittle. Similarly, at a higher strength of ECC, the stiffness of the connection also increases, which means that the flat plate becomes less capable of undergoing significant deformation before reaching its limit.

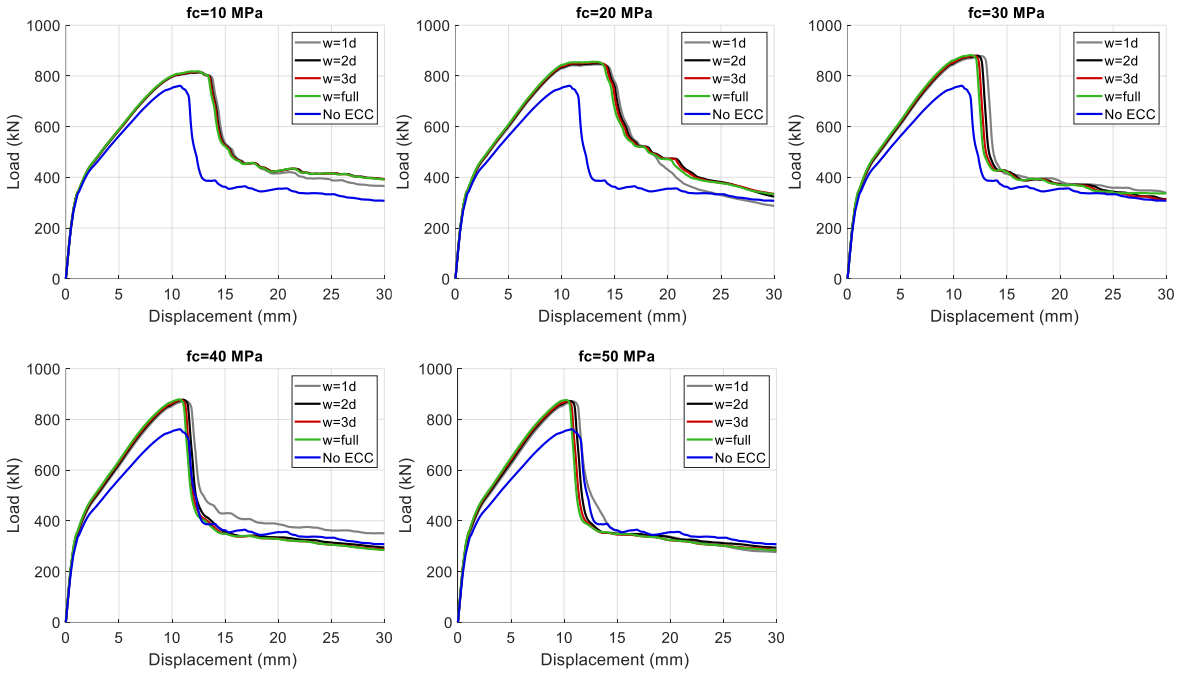

Figure 4.1. Global response of compression side retrofitting for different ECC strengths

4.1.2. Contribution of Concrete and ECC

Figure 4.2 demonstrates the contribution of each layer of concrete on punching shear strength of the flat plate model without ECC retrofitting along the distance from the column. It can be observed that the contribution of the first layer of concrete is significant around the column since the slab-column connection is under compression at this region. However, as the distance is further away from the column, the contribution of the first layers (Concr-1 and Concr-2) of concrete decreases significantly because the crack is inclined toward the tension zone of the slab. Thus, there is little concrete contribution from the compression zone to the resistance of the slab to punching shear at distances far from the column face. However, at a greater distance, the contribution of the layers at the tension zone of the slab increases. Thus, this confirms the punching shear failure mechanism that the shear crack is inclined and propagating from the tension zone to the compression zone.

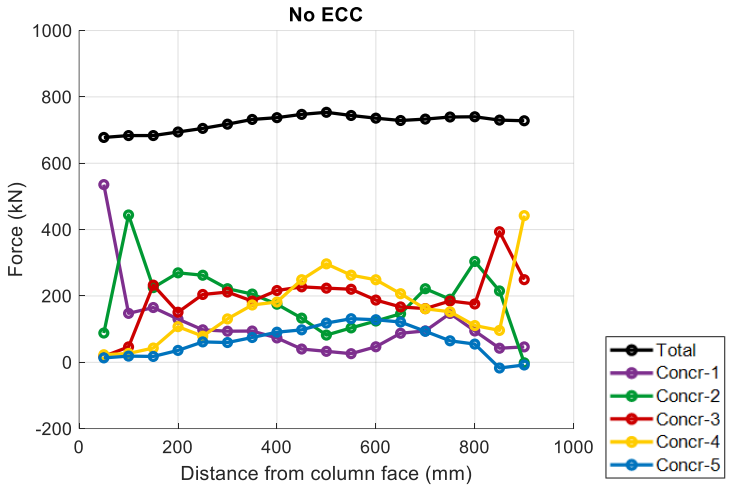

Figure 4.2. Contribution of each component of the model for control specimen without ECC

Figure 4.3. illustrates the contribution of concrete layers and ECC on the slab's compression surface with 30 mm thickness and 50 MPa strength to the shear resistance of the slab with varying ECC widths. In general, the contribution of the concrete follows the same trend as in the case of without retrofitting. However, the addition of ECC on the layer compression zone reduces the contribution of concrete adjacent to the slab-column joint by taking up most of the contribution by ECC. The punching shear contribution of ECC decreases as the distance from the column face gets larger. This demonstrates that increasing ECC width is not effective in enhancing the flat plate's punching shear resistance. Therefore, it is clear that the punching shear response of the flat plate strengthened with ECC remains unchanged when the width is increased from 1d to full slab length.

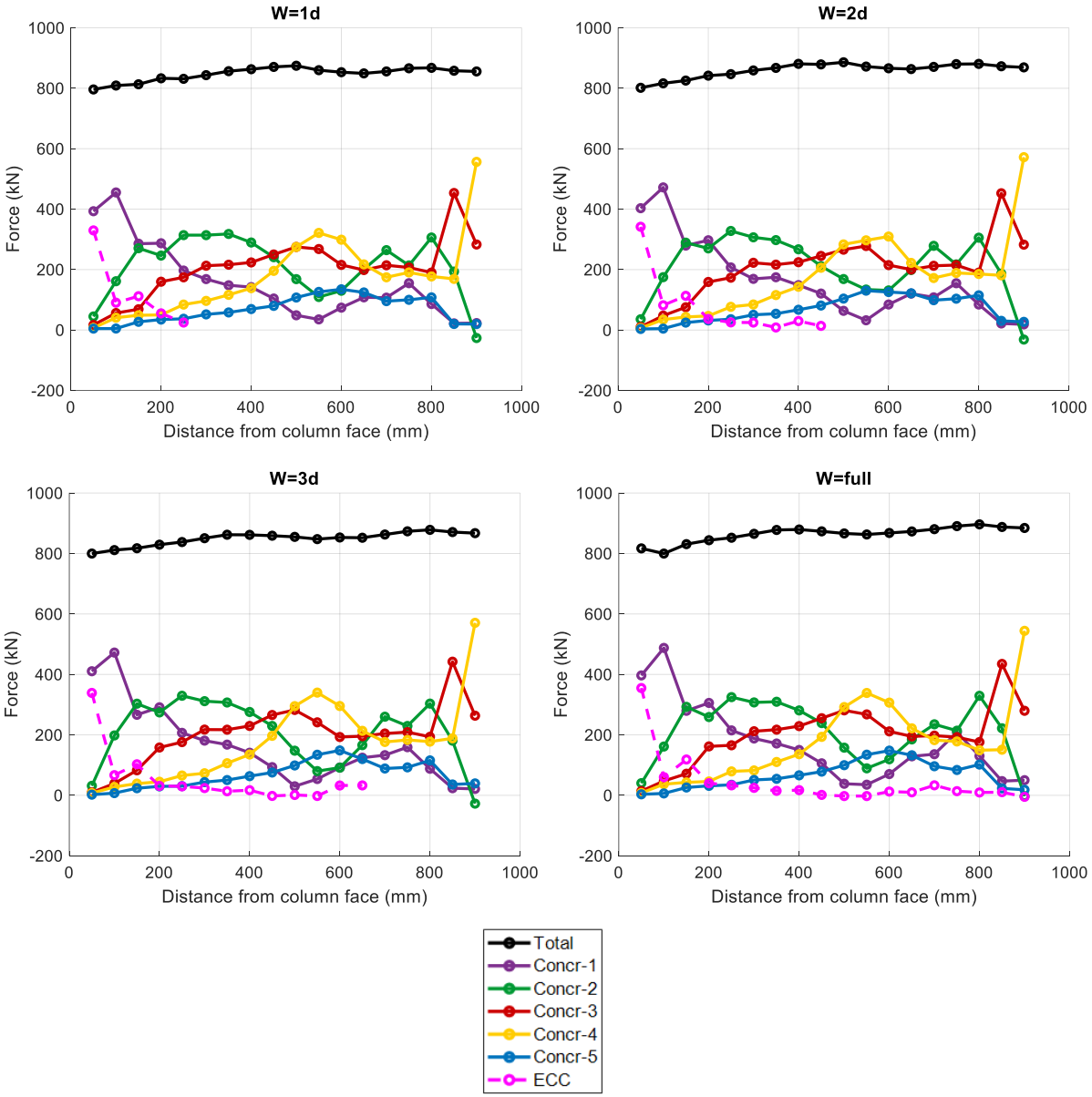

Figure 4.3. Contribution of each component of the model with 30mm, 20MPa ECC on the compression side of a slab.

Figures 4.4 to 4.6 demonstrate the global response plots for concrete and ECC contributions with different ECC strengths at locations 50mm (0.23d), 100mm (0.46d), and 250mm (1.15d) away from the slab-column joint. The load-displacement curve at $f_{c0} = 0$ corresponds to the unretrofitted flat plate model. It is noticeable that the contribution of concrete near the joint of the slab and column is less compared to the model without ECC retrofit since the considerable shear contribution is produced from the ECC layer added on the compression side of the slab. Furthermore, it is noticed that the shear resistance contribution of ECC increases for strengths from 10 to 30 MPa, after which it remains constant. This indicates that despite the increase in compressive strength of ECC, its contribution to punching shear

resistance is limited. As the distance increases further away from the slab-column joint, the major shear strength contribution is generated from concrete, while the ECC contribution reduces.

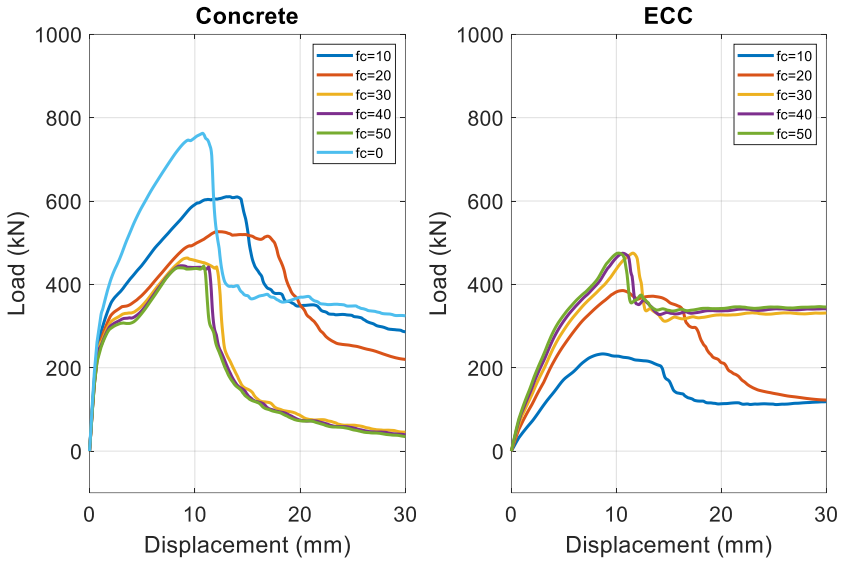

Figure 4.4. Shear strength contribution of ECC and concrete of the slab with 30mm 20MPa ECC at 0.23d (50mm)

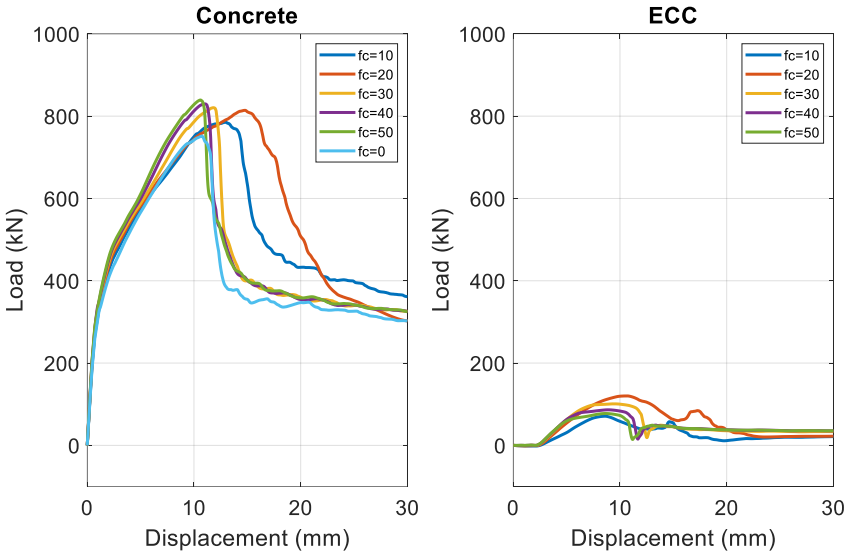

Figure 4.5. Shear strength contribution of ECC and concrete of the slab with 30mm 20MPa ECC at 0.46d (100mm)

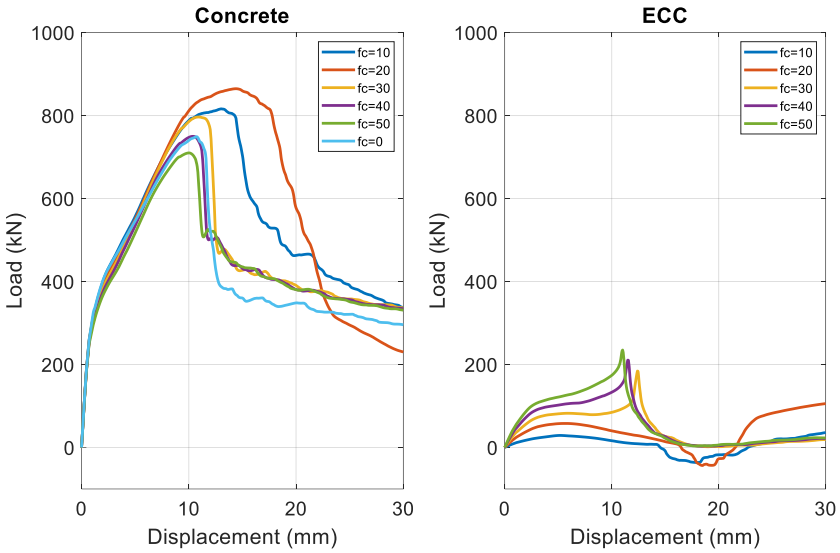

Figure 4.6. Shear strength contribution of ECC and concrete of the slab with 30mm 20mpa ECC at 1.15d (250mm)

4.1.3. Cracking pattern

This section presents the cracking patterns of the flat plate models with ECC on the slab's compression side. The maximum principal equivalent plastic tensile strain contour plots are used to illustrate the cracking pattern of the flat plate in ABAQUS. Figure 4.7 compares the maximum principal plastic strain of flat plates without and with ECC retrofit under the maximum load. The column is white since the material definition was elastic, thus no plastic strain is exhibited. The grey color indicates the cracked region.

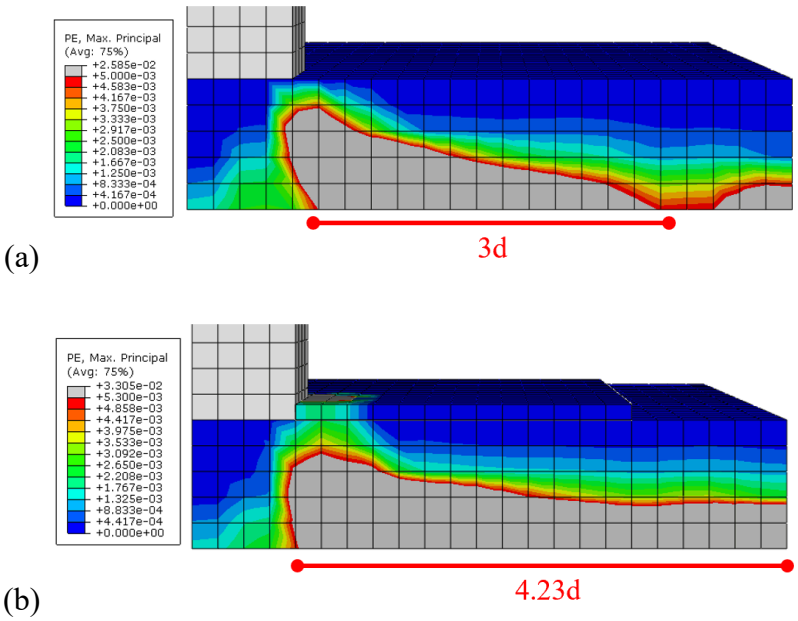

Figure 4.7. The cracking pattern of a flat plate (a) without ECC and (b) with ECC at peak load.

Figure 4.7a demonstrates the cracking pattern of the unretrofitted flat plate at peak load. The distance of the tension crack is 650 mm which corresponds to the 3d distance from the slab-column joint. Moreover, the crack is inclined toward the compression zone, indicating the punching shear failure.

At the peak strength, large tensile stresses were developed on the tension zone, thus damaging almost the entire slab face (Figure 4.7b). Furthermore, it is observed that the crack is mainly distributed on the tension surface of the slab and are mainly flexural cracks. Since cracks initiate from the tension zone of the slab, retrofitting on the compression side was not effective in lessening the crack distribution from the tension side. However, the cracks adjacent to the column are getting inclined and propagating toward the compression zone. Thus, the higher maximum principal strain can be observed at the corner of the ECC layer. This confirms that the ECC retrofitting provides additional resistance to the slab-column joint, which was covered in the previous section.

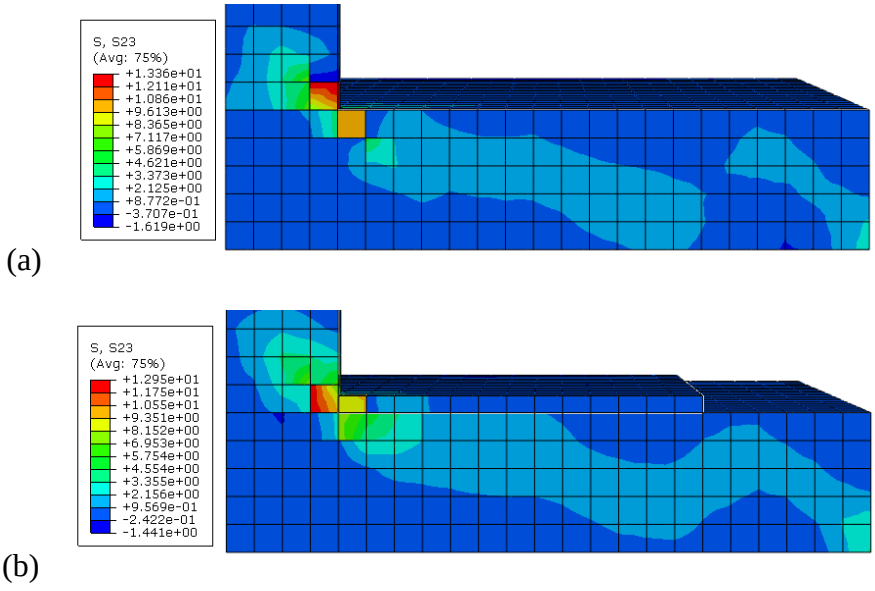

Figure 4.8. The shear stress profile of a flat plate (a) without ECC and (b) with ECC at peak load.

Figure 4.8 illustrates the comparison of the shear stress propagation along the thickness and length of the slab. In general, the shear stress is spread diagonally along the slab thickness with the maximum shear stress concentrated at the slab-column joint on the compression zone. As it was mentioned in the previous section (Section 4.1.2), when the ECC is added on the compression side, the first layer of the concrete and ECC layer experience the highest shear stress at the slab-column joint location. This demonstrates the importance of adding the ECC layer on the compression side of the slab to resist higher punching strength.

4.2. Tension side retrofitting

4.2.1. Global response

Figure 4.9 illustrates the global load versus displacement response of a flat plate with varying ECC compressive strengths from 10 to 50 MPa and widths from 1d to full slab length. Overall, it is clear that ECC strengthening from the tension side provides additional punching shear resistance to a flat plate. It should be noted that ECC with widths of 1d and 2d does not impact the punching shear strength. This might be since the critical perimeter of the flat plate is more than 2d. Furthermore, the higher the strength of ECC, the greater the punching shear response and stiffness.

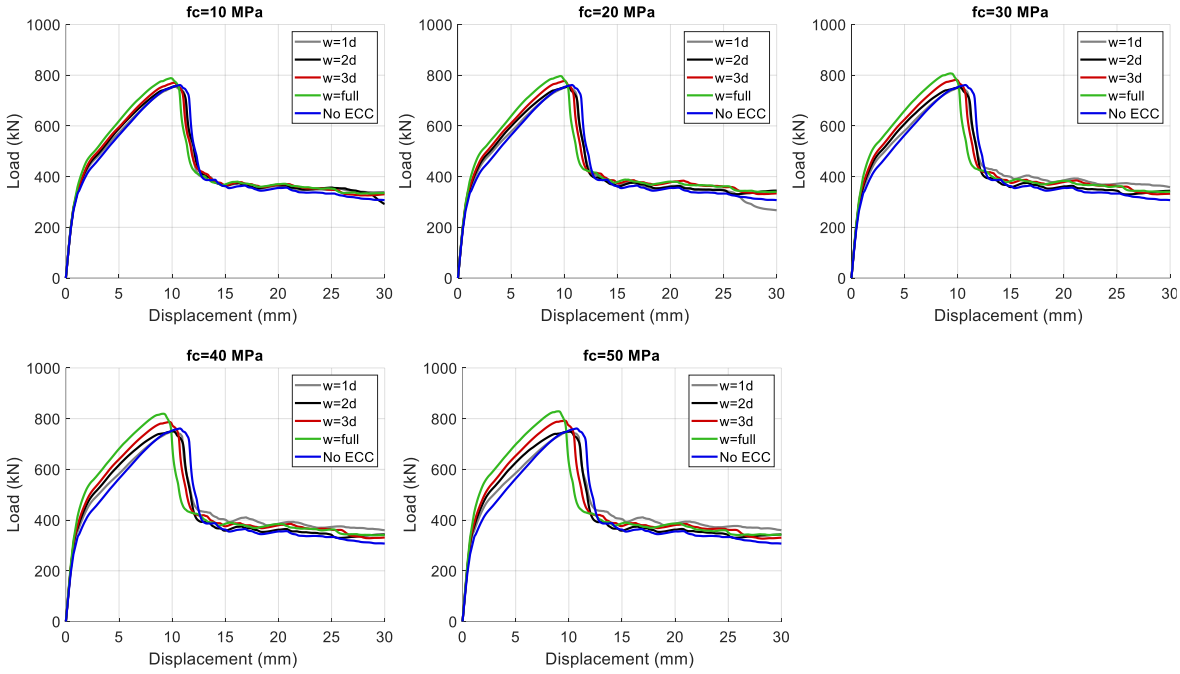

Figure 4.9. Global response of tension side retrofitting for different ECC strengths

4.2.2. Contribution of Concrete and ECC

Figures 4.10 to 4.14 demonstrate the global response plots for concrete and ECC contributions with different ECC strengths at locations 50mm (0.23d), 250mm (1.15d), 450mm (2.07d), 650mm (3), and 950mm (4.15d) away from the column face. Overall, ECC has no direct shear contribution, however, adding an ECC layer on the slab's tension side increased the contribution of the concrete throughout the whole distance from the column compared to the slab without retrofitting. This might be because the neutral axis shifted downward due to the additional layer in the slab which resulted in an enlarged compression zone of the slab. Therefore, the ECC layer enhances the global punching shear response of the slab. As the distance from the slab-column connection is greater, the contribution of the ECC becomes

negative, thus increasing the concrete contribution and maintaining the force equilibrium of the system. Moreover, with the rise of the strength of the ECC, the contribution of concrete also increases, becoming stiffer and more brittle.

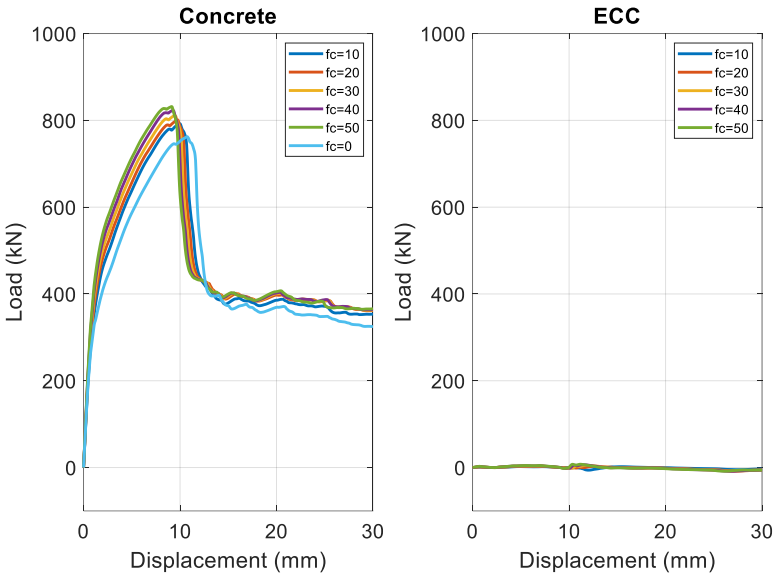

Figure 4.10. Shear strength contribution of Concrete and ECC of slab with 20mm 50mpa ECC at 0.23d

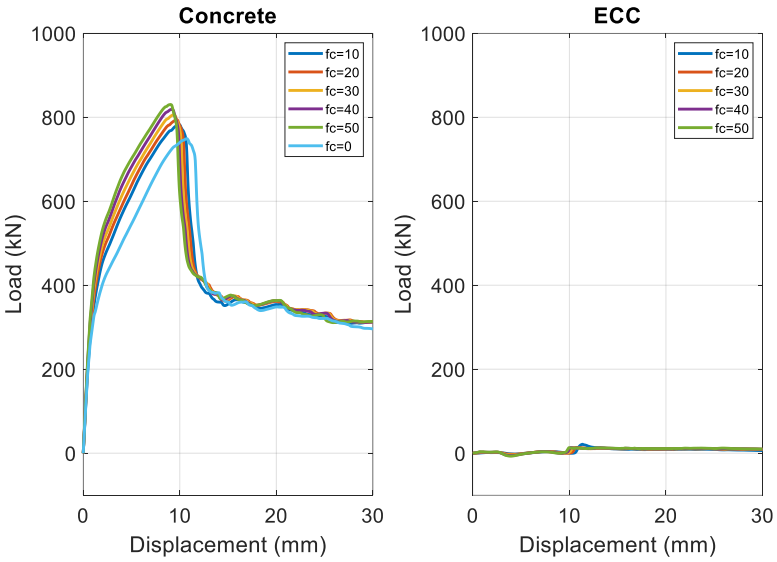

Figure 4.11. Shear strength contribution of Concrete and ECC of slab with 20mm 50mpa ECC at 1.15d

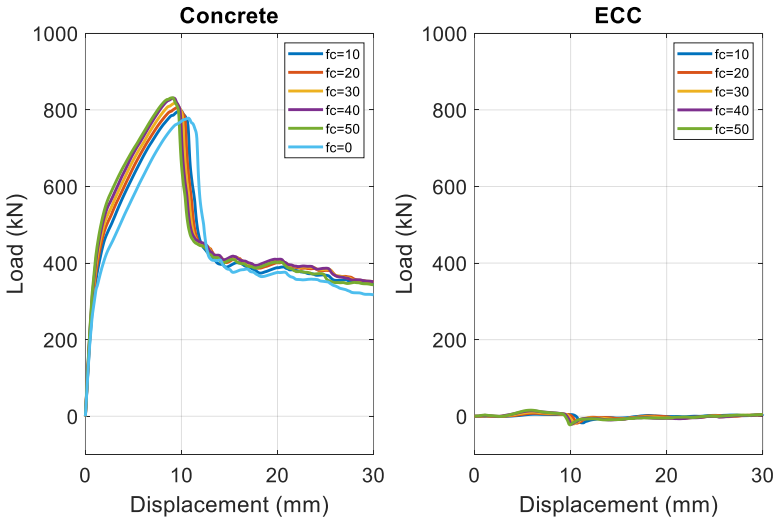

Figure 4.12. Shear strength contribution of Concrete and ECC of slab with 20mm 50mpa ECC at 2.07d

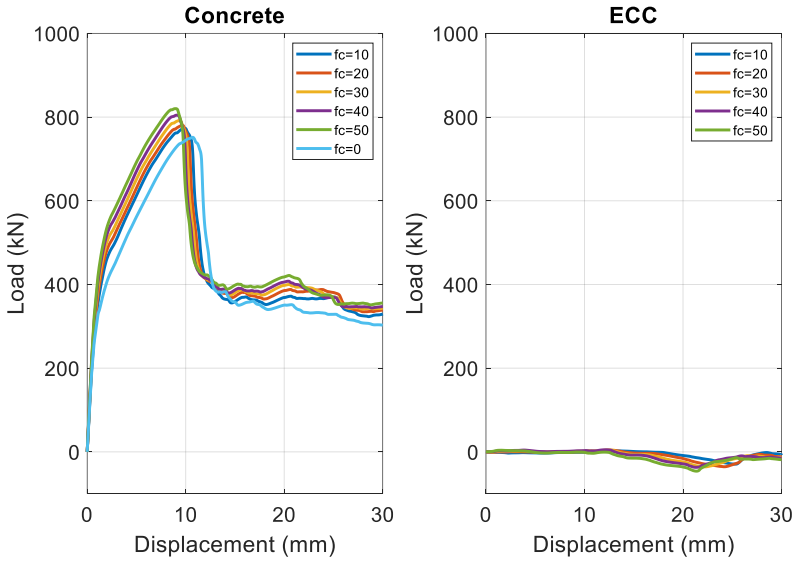

Figure 4.13. Shear strength contribution of Concrete and ECC of the slab with 20mm 50mpa ECC at 3d

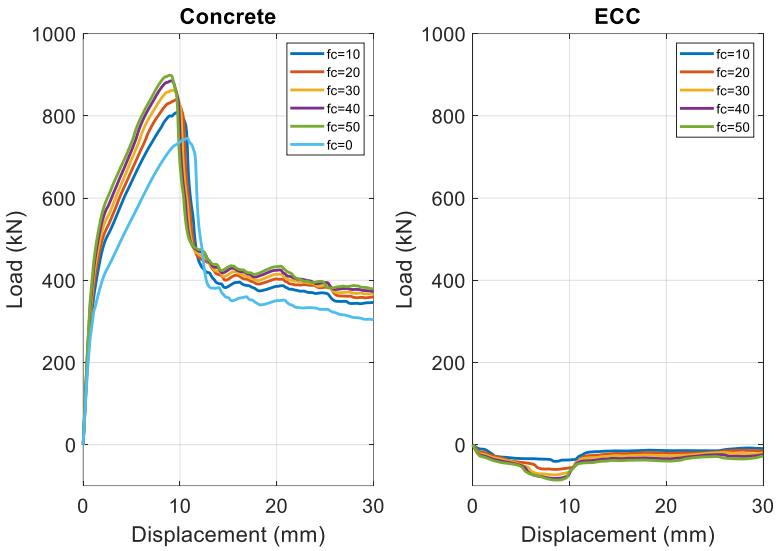

Figure 4.14. Shear strength contribution of Concrete and ECC of slab with 20mm 50mpa ECC at 4.15d

Figure 4.15 illustrates the contribution of concrete layers and ECC on the tension side of the slab with 20 mm thickness and 50 MPa strength to the punching shear capacity of the slab with varying ECC widths along the length of the slab. In general, the contribution of the concrete follows the same trend as in the case of without retrofitting (Figure 4.2). Furthermore, ECC on the tension side has no direct contribution or the effect is very low toward the punching shear resistance. It should be noticed that as the distance from the column is greater, the contribution of the bottom layers of the slab is getting higher. The flat plate model with 1d and 2d width ECC retrofit produces almost identical results, while the response of flat plate with 3d and full slab width retrofit is somewhat greater because of the increased contribution from concrete and a modest contribution from the ECC layer.

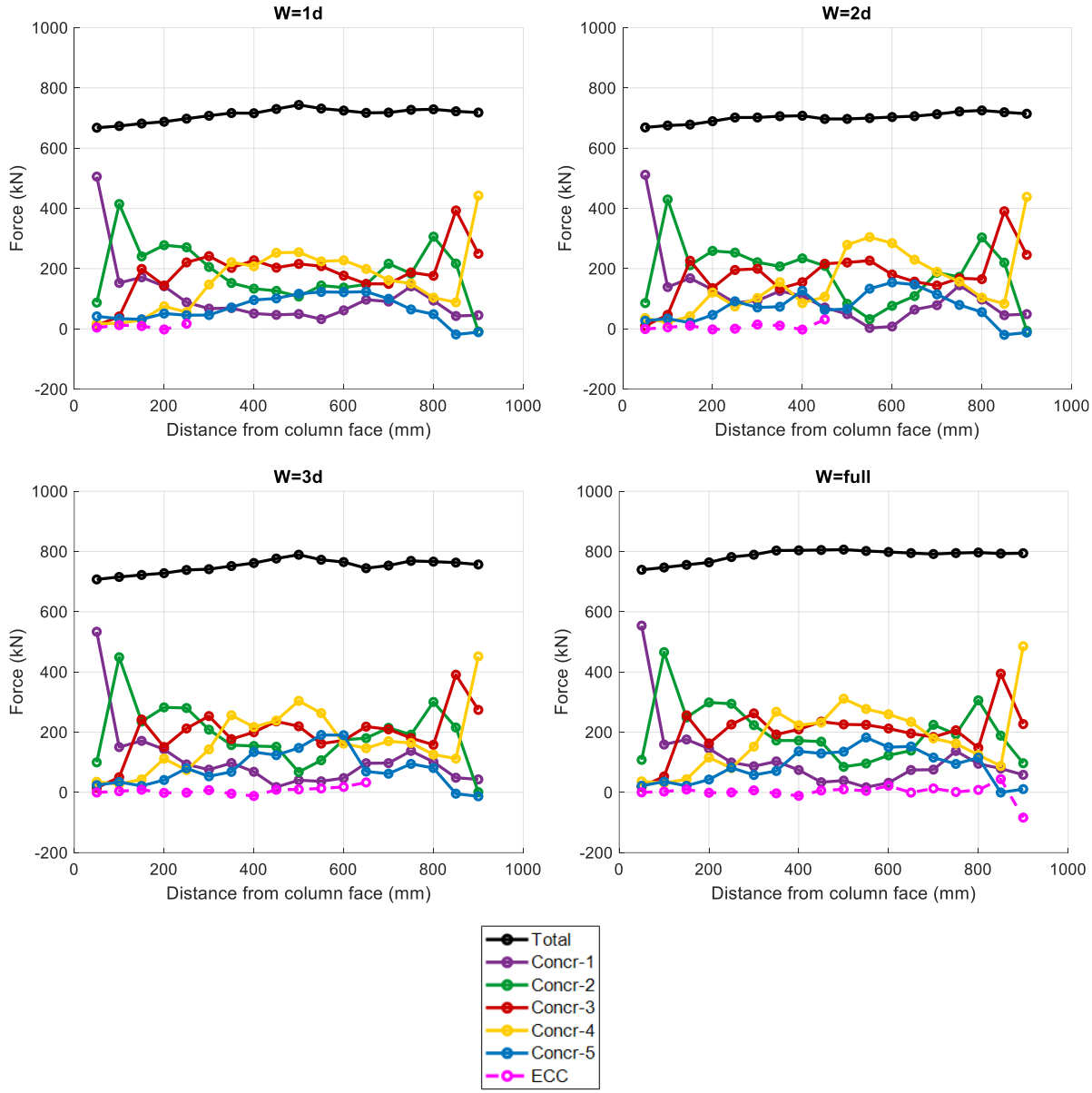

Figure 4.15. Contribution of each component of the model with 20mm, 50MPa ECC on the tension side of a slab.

4.2.3. Cracking pattern

This section presents the cracking patterns of the flat plate models with ECC on the slab's tension side. Similarly, the maximum principal equivalent plastic tensile strain contour plots are used to demonstrate the cracking pattern of the flat plate. Figure 4.16 shows the maximum principal equivalent plastic strain of flat plates with 1d, 2d, 3d, and full slab width ECC retrofit under the maximum load.

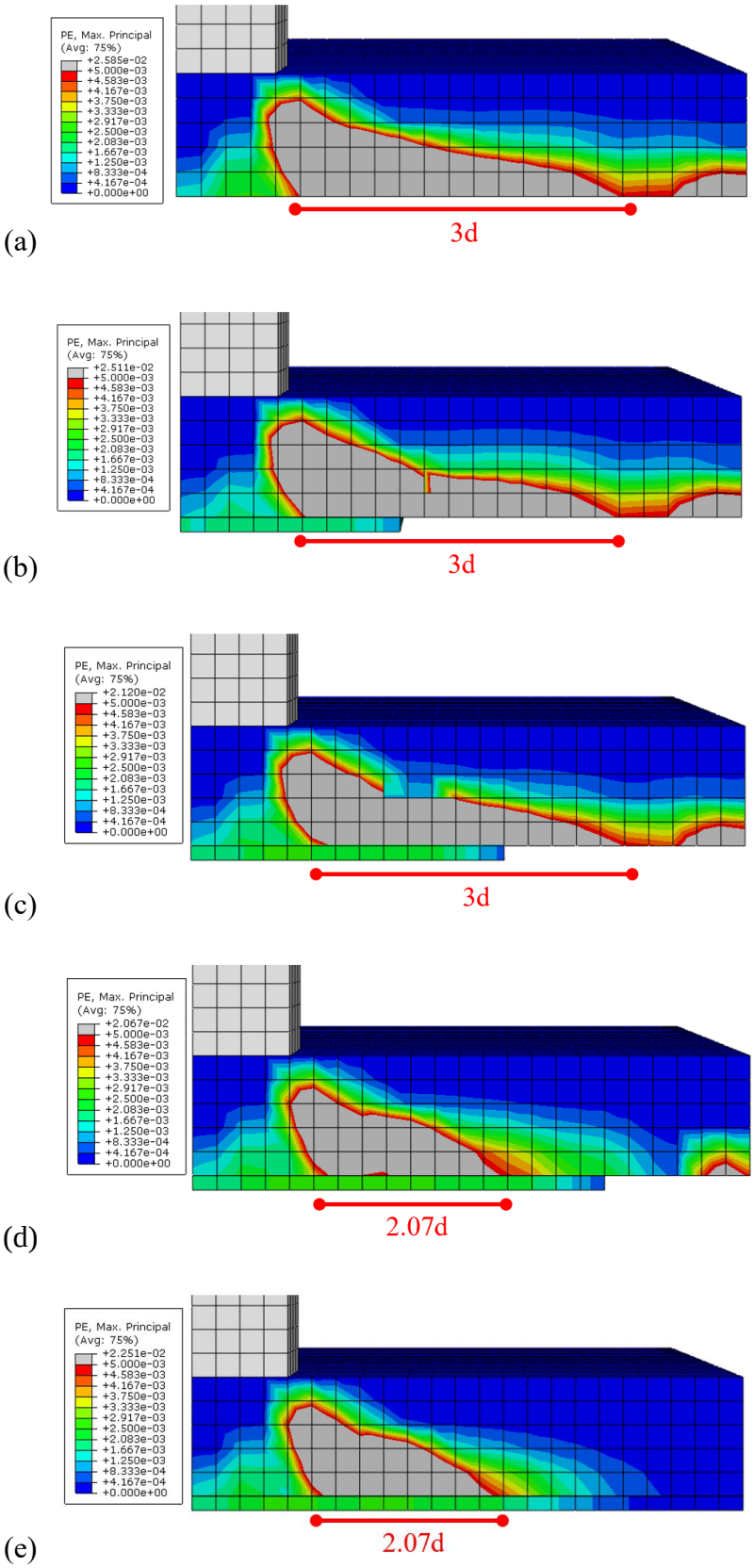

Figure 4.16. The cracking pattern of a flat plate with ECC on the tension side at peak load for ECC with (a) without, (b) 1d, (c) 2d, (d) 3d, and (e) full slab width.

Figures 4.16b and 4.16c demonstrate the cracking pattern of the flat plate with 1d and 2d ECC retrofitting from the tension side of the slab. First, the damaged area of the concrete is almost a 3d distance from the column, which is similar to the unretrofitted model (Figure 4.16a). Moreover, the whole area of the 2d width ECC is experiencing a plastic strain. This confirms that ECC with less width than the critical perimeter of the slab is not effective in damage-controlling.

It is clear from the contour plots of the flat plate with 3d width ECC retrofitting (Figure 4.16d) that ECC retrofit on the tension side reduced the damaged area of the flat plate. This demonstrates that strengthening a flat plate with ECC on the tension side might decrease the critical perimeter of the cracking region. The comparison of the 3d and full slab width ECC retrofitting shows that full slab width is more effective in controlling the damage propagation. Moreover, the diagonal cracking is observed where the crack propagates toward the compression zone; thus, the double-sided retrofitting is discussed in the next section to resist the punching load from the compression side of the slab.

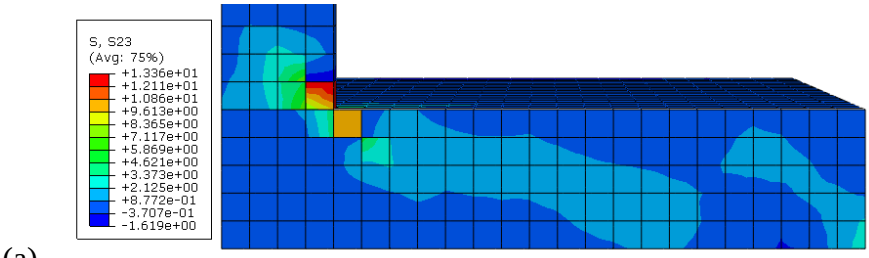

(a)

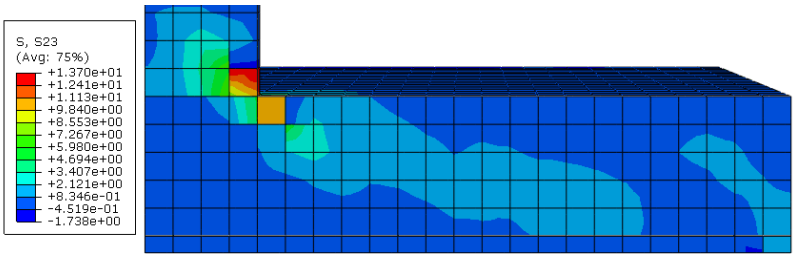

(b)

Figure 4.17. The shear stress profile of a flat plate (a) without ECC and (b) with ECC at peak load.

Figure 4.17 demonstrates the shear stress propagation along the thickness of the slab. The shear stress is distributed diagonally, indicating the inclined shear crack. Overall, both unretrofitted and retrofitted models follow the same trend. As discussed in the previous section, ECC retrofitting from the tension side has no direct shear contribution but compared with the unretrofitted model, the retrofitted slab is experiencing a little higher shear stress. The highest shear stress is found on the compression zone at the joint of the slab with the column.

4.3. Double-sided retrofitting

4.3.1. Global response

The global response plots for the flat plate retrofitted from both sides of the slab with varying ECC strengths from 10 to 50 MPa and widths from 1d to full slab are presented in Figure 4.18. It is observed that both-sided ECC retrofit considerably enhances the punching shear response of the flat plate in comparison to single-sided retrofitting. The deformation capacity of the flat plate increases until ECC strength reaches 20 MPa, after which it reduces. The deformation capacity contribution is mainly generated from the compression side retrofitting. Furthermore, the punching shear resistance augments as the ECC strength increases from 10 to 50 MPa. In addition, it must be noted that the obtained strength of the double-sided retrofitted slab is not the result of the superposition principle since the peak strengths of the compression and tension-sided-retrofitted model happen at different displacements.

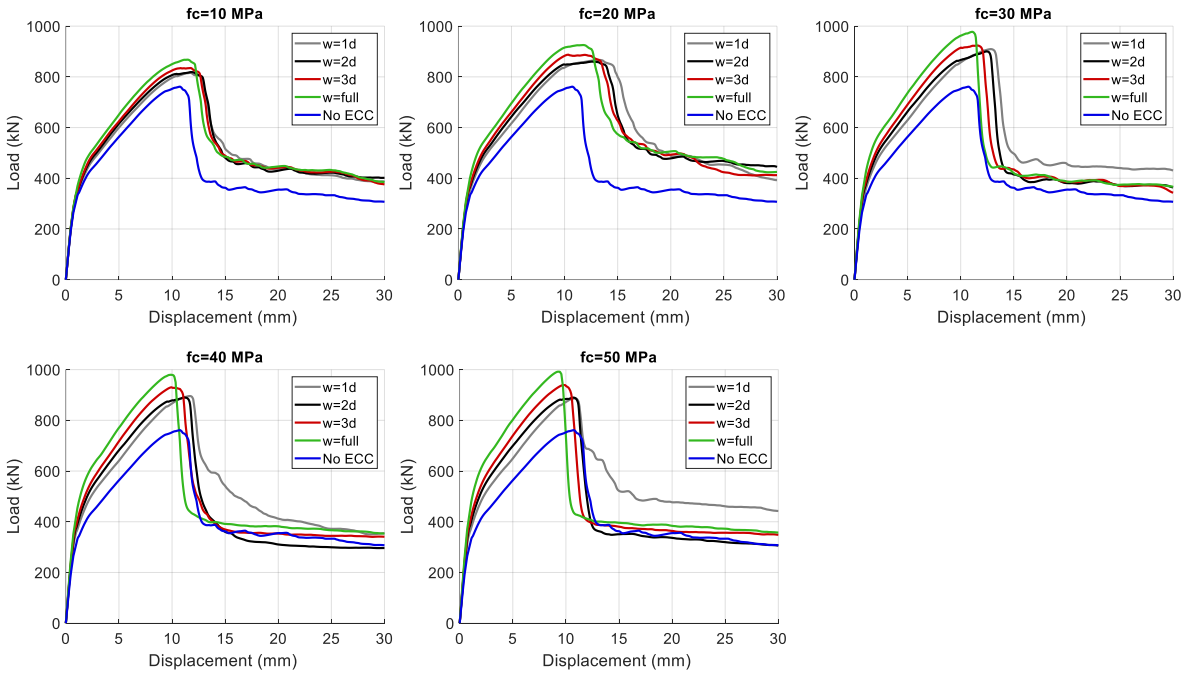

Figure 4.18. Global response of both-sided retrofitting for different ECC strengths

4.3.2. Contribution of Concrete and ECC

The contribution plot for concrete and ECC is presented in Figure 4.19. It can be observed that ECC on the compression side generates the highest response and is increased as the ECC gets wider. Even though the direct shear contribution of ECC from the tension face is very little, it considerably improves the response of the concrete layers, thus enhancing the global response of the flat plate model under punching load. Accordingly, the combined effect

of the ECC from the tension and compression face significantly improves the punching shear resistance of a flat plate compared to single-sided retrofitting.

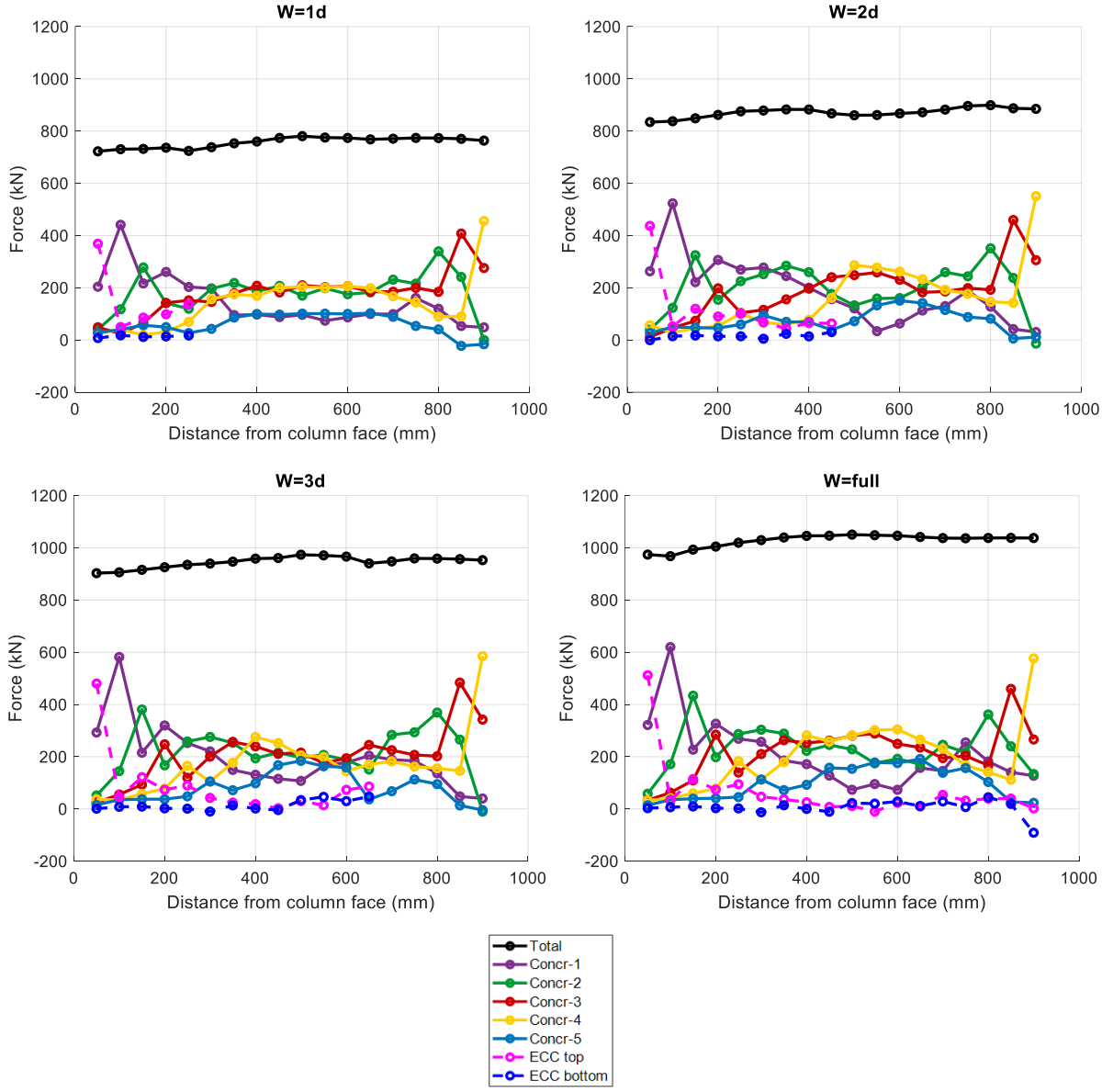

Figure 4.19. Contribution of each component of the model with 30mm, 50MPa ECC on both sides of a slab.

Figures from 4.20 to 4.24 show the global response plots for concrete and ECC contributions with different ECC strengths at locations 50mm (0.23d), 250mm (1.15d), 450mm (2.07d), 650mm (3d), and 950mm (4.15d) far from the slab-column joint. Overall, it is obvious that the layer of ECC applied on the compression face contributes the highest near the slab-column joint since this is the region that experiences the greatest shear stress. However, as the distance from the column becomes larger, the contribution of ECC on the compression side

reduces significantly. On the contrary, ECC on the tension side has no direct shear strength contribution but it considerably enhances the contribution of concrete.

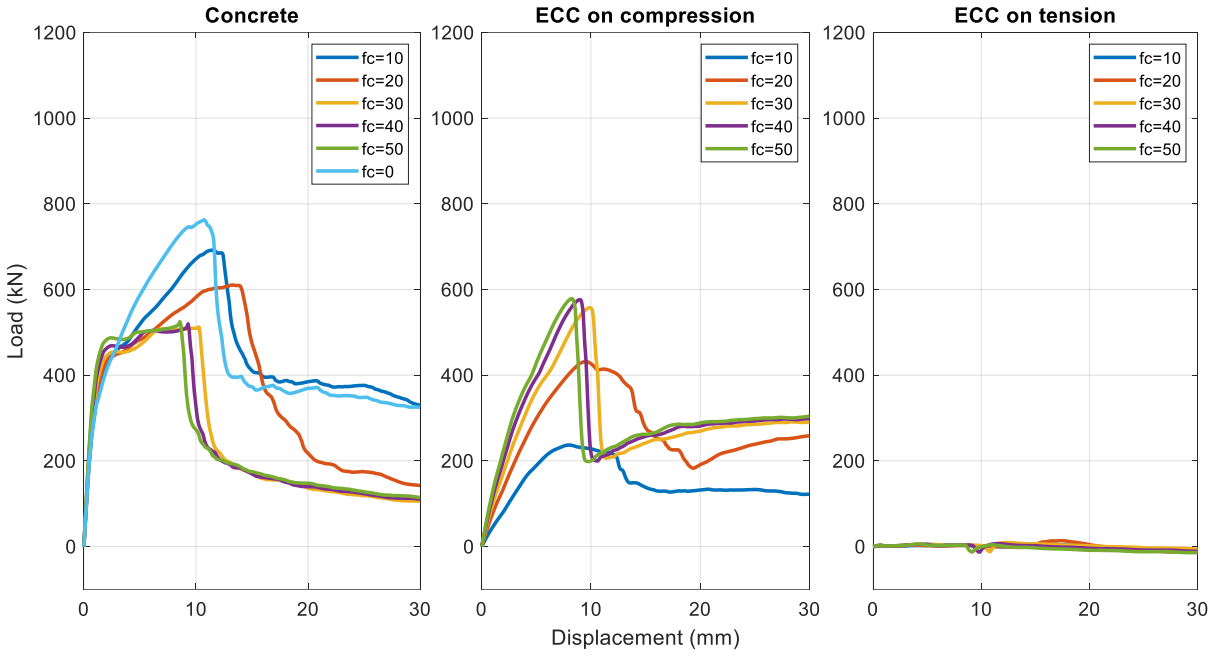

Figure 4.20. Shear strength contribution of Concrete and ECC of the slab with 30mm 50mpa ECC at 0.23d

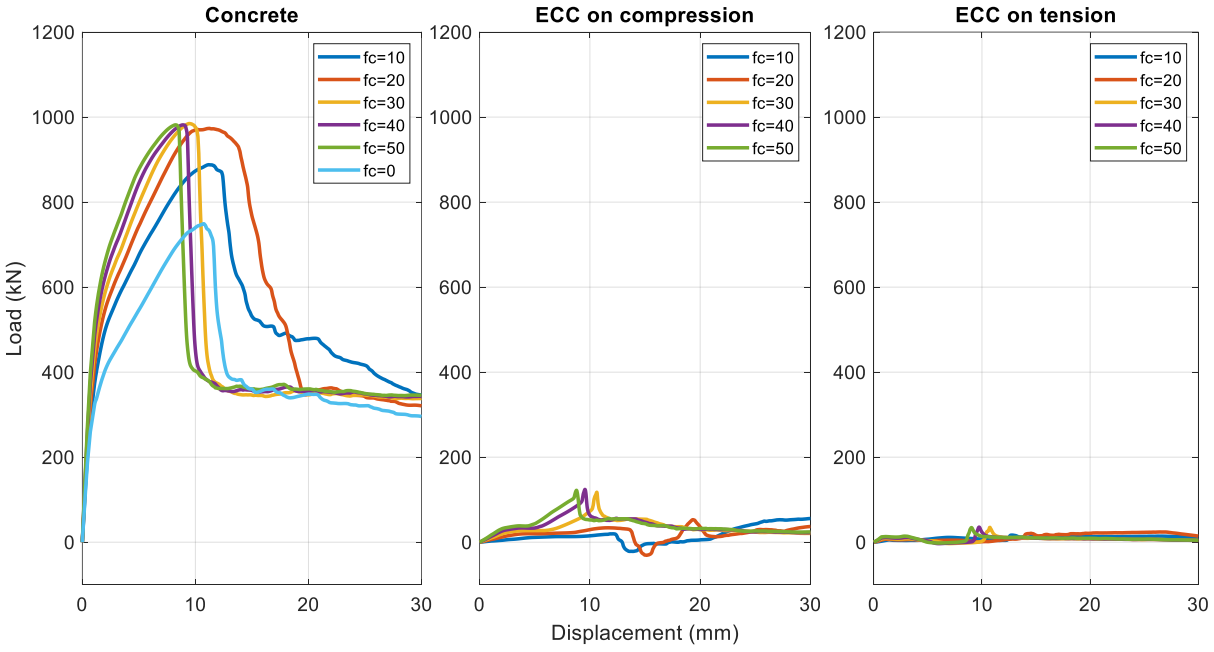

Figure 4.21. Shear strength contribution of Concrete and ECC of the slab with 30mm 50mpa ECC at 1.15d

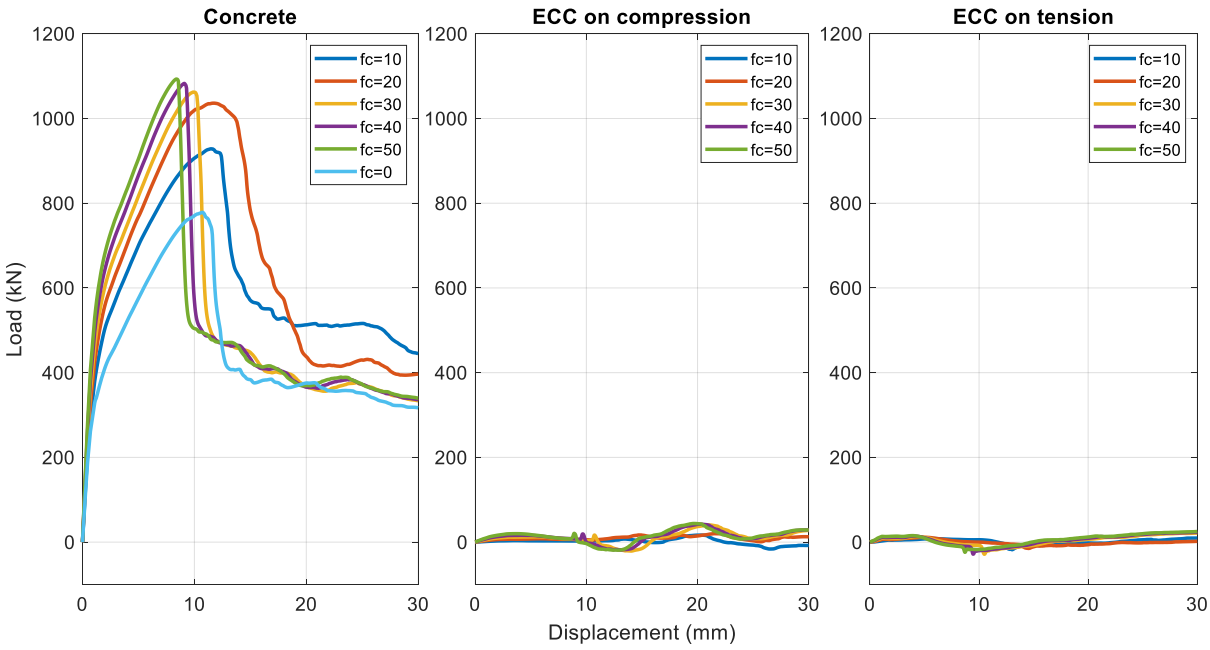

Figure 4.22. Shear strength contribution of Concrete and ECC of the slab with 30mm 50mpa ECC at 2.07d

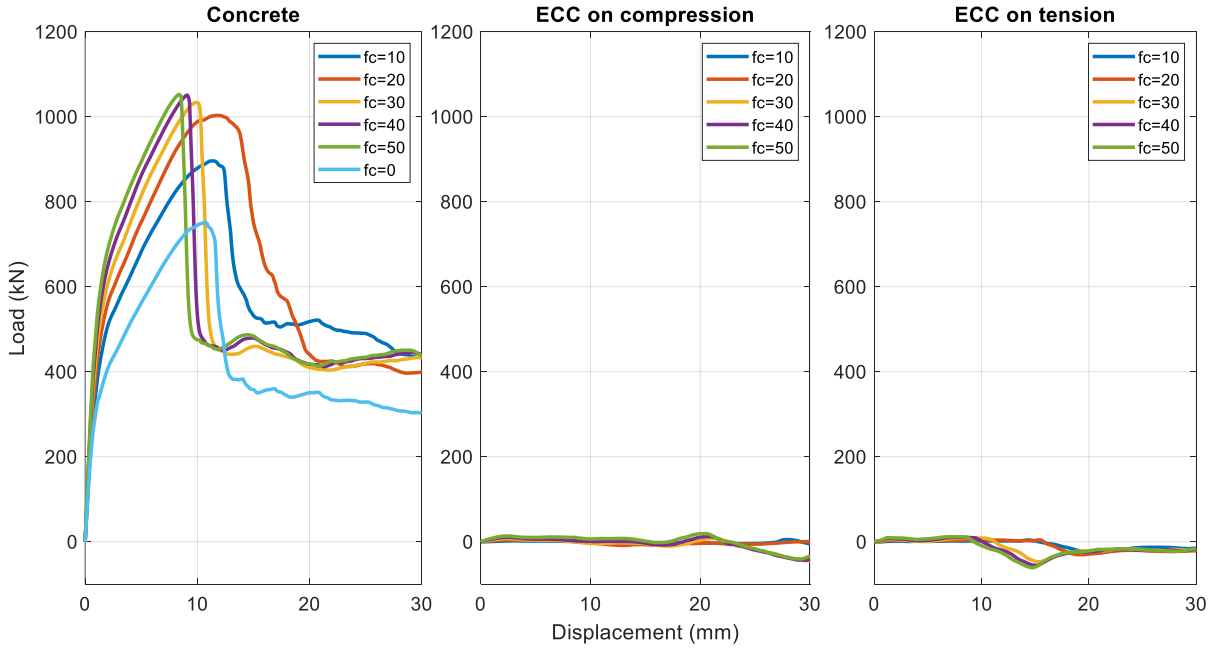

Figure 4.23. Shear strength contribution of Concrete and ECC of the slab with 30mm 50mpa ECC at 3d.

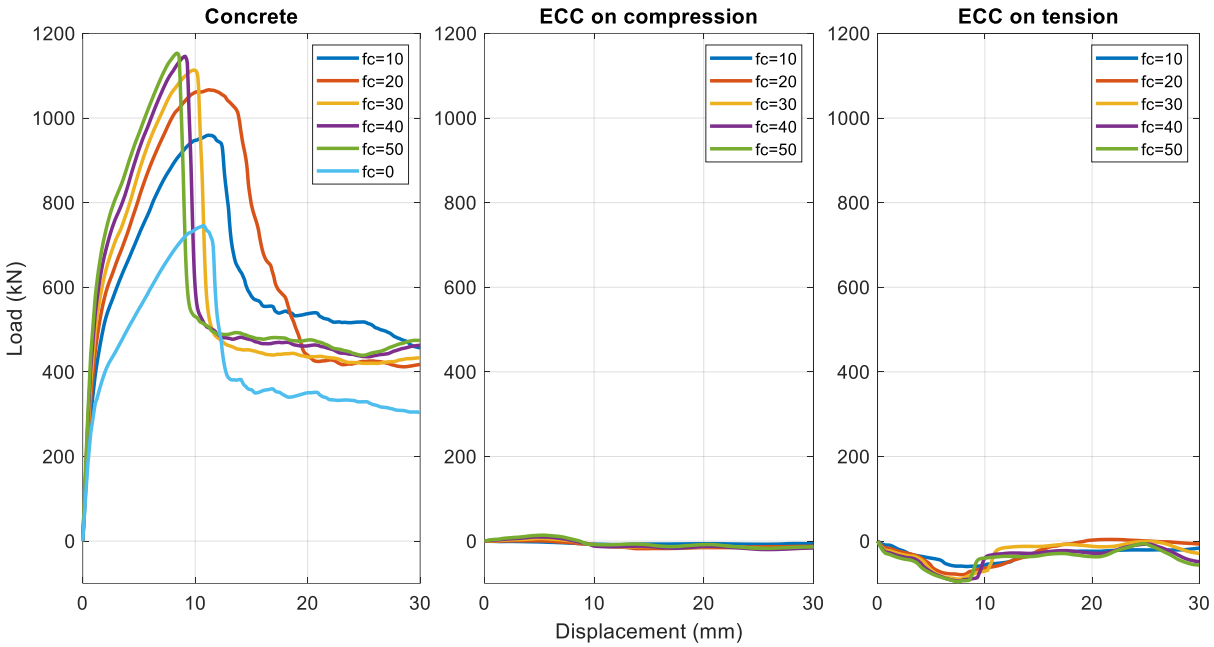

Figure 4.24. Shear strength contribution of Concrete and ECC of the slab with 30mm 50mpa ECC at 4.15d

4.3.3. Cracking pattern

Figure 4.25 presents the cracking pattern of the flat plate retrofitted with ECC from both sides. Similar to the single-sided retrofitted flat plate models, the maximum equivalent tensile plastic strain contour plot is generated. It can be observed that the tension side retrofitting reduces the damaged area of the slab, thus confirming the importance of tension side retrofitting for damage control. Moreover, the inclined crack is propagated to the compression zone, which is eventually controlled by the ECC layer on the compression side.

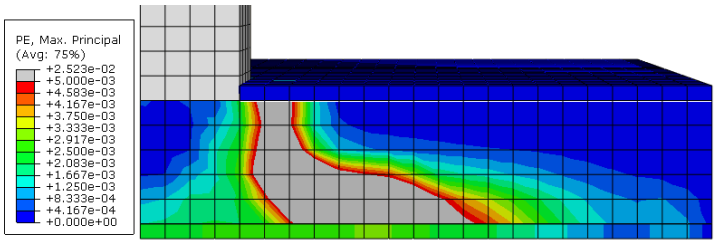

Figure 4.25. The cracking pattern of a flat plate with full-width ECC on both sides at peak load.

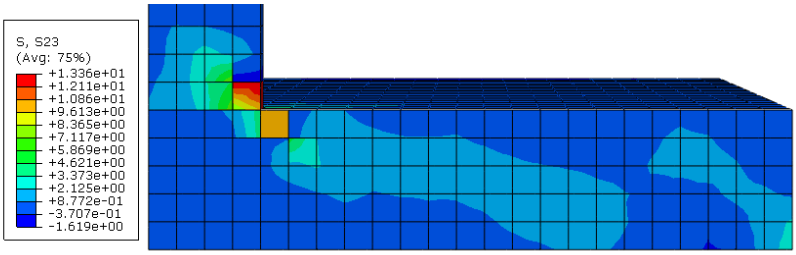

(a)

(b)

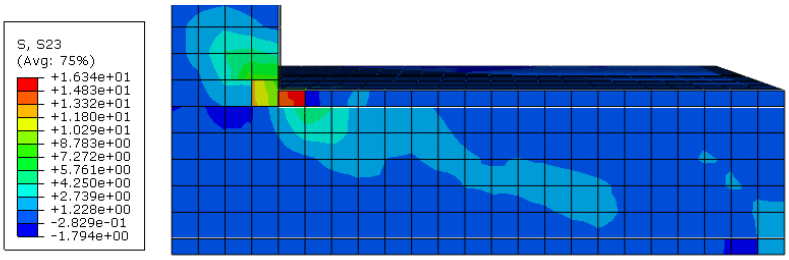

Figure 4.26. The shear stress profile of a flat plate (a) without ECC and (b) with ECC at peak load.

The shear stress profile (Figure 4.26) shows that a double-sided retrofitted flat plate can withstand the highest shear stress of almost 16 MPa. The shear stress is concentrated at the place of the failure that is the slab-column joint on the compression side. Moreover, due to retrofitting from both sides retrofitting, the propagation of the shear stress to the entire profile is confined. Thus, double-sided retrofitting is crucial to control the damage propagation and improve the strength of the connection.

4.3.4. Misaligned retrofitting

The obtained results from the previous section suggest that the response of the compression-sided retrofitting is independent of the ECC width. Similarly, tension-sided retrofitting is effective when the ECC width is 3d or more. Therefore, in this section, the misaligned double-sided retrofitting is discussed. For that purpose, numerical simulations were carried out with only a 250mm (1d) width ECC compressive strengthening and varying tensile retrofitting with 250 mm (1d), 450mm (2d), 650mm (3d), and 950mm (full slab) widths. Figure 4.27 presents the global load versus displacement response of flat plate retrofitted on both sides with misaligned retrofitting. In general, the misaligned retrofitting with constant 1d width ECC on the compression side generates almost the same results as the double-sided retrofitting covered in the previous section (Section 4.3.1).

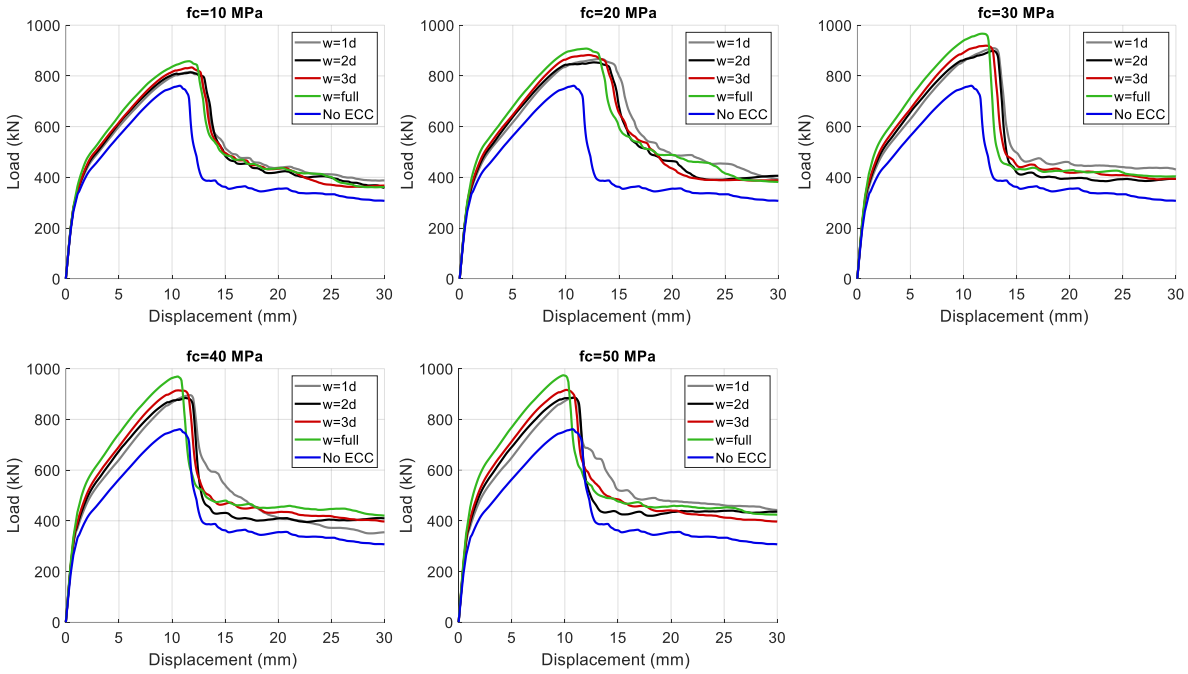

Figure 4.27. Global response of both-sided misaligned retrofitting for different ECC strengths

To better represent the response of the misaligned retrofitting the following parametric plot on the peak strengths of flat plates with full slab width tensile side retrofitting and 1d and full slab length width retrofitting on the compression side is presented in Figure 4.28, where the C represents compression side and T represents the tension side. As expected, both 1d and full slab width ECC retrofitted flat plates follow the same trend with varying ECC compressive strengths. However, the peak strength of the model with a full slab width ECC on the compression side is 4% greater than the peak strength of the slab with 1d width ECC on the compression side. That indicates that even though single-sided compression retrofitting remains independent of the width increase of the ECC, under the combined strengthening the strength of the flat plate increases with the ECC width.

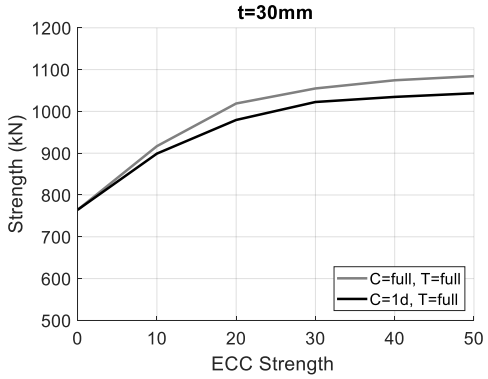

Figure 4.28. Peak strength of both-sided misaligned retrofitting for different ECC strengths

4.4 Parametric results

4.4.1. Effect of ECC parameters on compression side retrofitting

In this section, the result of the parametric study is discussed, considering the effects of ECC strength, thickness, width, and location on the punching shear strength of the flat plate. Figure 4.29 demonstrates the peak strength of flat plates with compression side retrofitting for different ECC strengths and widths with thicknesses of 15mm, 20mm, 25mm, and 30mm. The peak strength of the unretrofitted flat plate corresponds to the data point where the ECC width is equal to 0. As seen, the peak strength of the flat plate increases only when the 1d width ECC is added to the model with an increase of 5-21% in strength, confirming an ineffectiveness of ECC width increase. The highest strength of 922.2 kN was obtained by the flat plate model retrofitted with 30mm and 50 MPa ECC, which shows a 21% difference from the unretrofitted model with 764.56kN strength. It is also noticed that the peak strength of flat plates augments with higher compressive strength and greater thickness. However, for ECC strengths from 30 to 50 MPa, the strengths of flat plates remain constant.

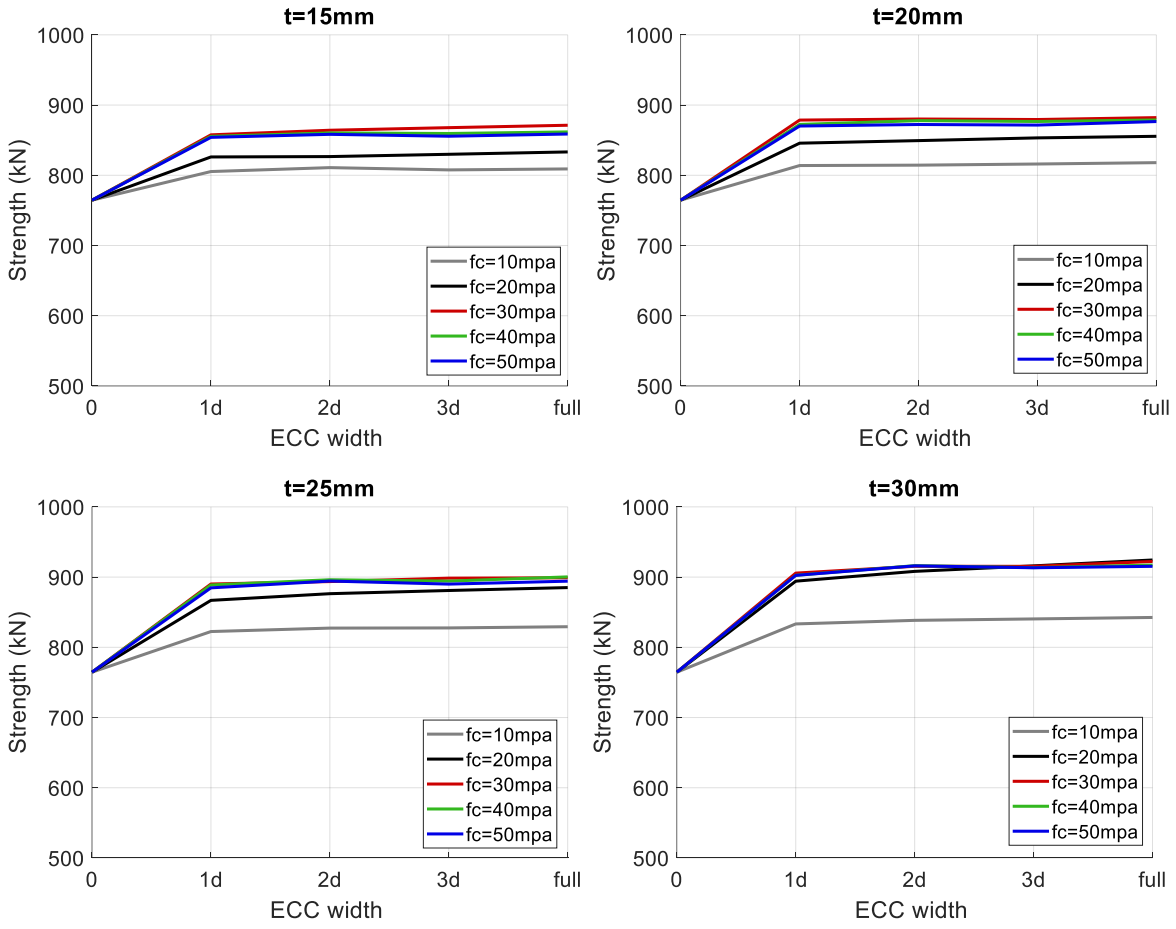

Figure 4.29. Peak strength of flat plate for different ECC strengths and widths with thicknesses of 15mm; 20mm; 25mm; and 30mm.

Figure 4.30 provides the deformation capacity of flat plates for different ECC strengths and widths with thicknesses of 15mm, 20mm, 25mm, and 30mm. The deformation capacity is not consistent for different ECC strengths. For the ECC strengths of 10 to 30 MPa, the deformation capacity of the flat plates increases when compared to the unretrofitted model. However, at a greater strength of 40 and 50 MPa, the deformation capacity is reduced. Overall, the deformation capacity is constant despite the ECC width increase. However, there is a sudden drop for the model with 20 MPa and 15mm ECC with 3d width. This drop might happen due to early failure of the concrete under concentrated load. According to the plots, the low-strength ECC in the range of 10 to 20 MPa is more effective for increasing the deformation capacity of the flat plate.

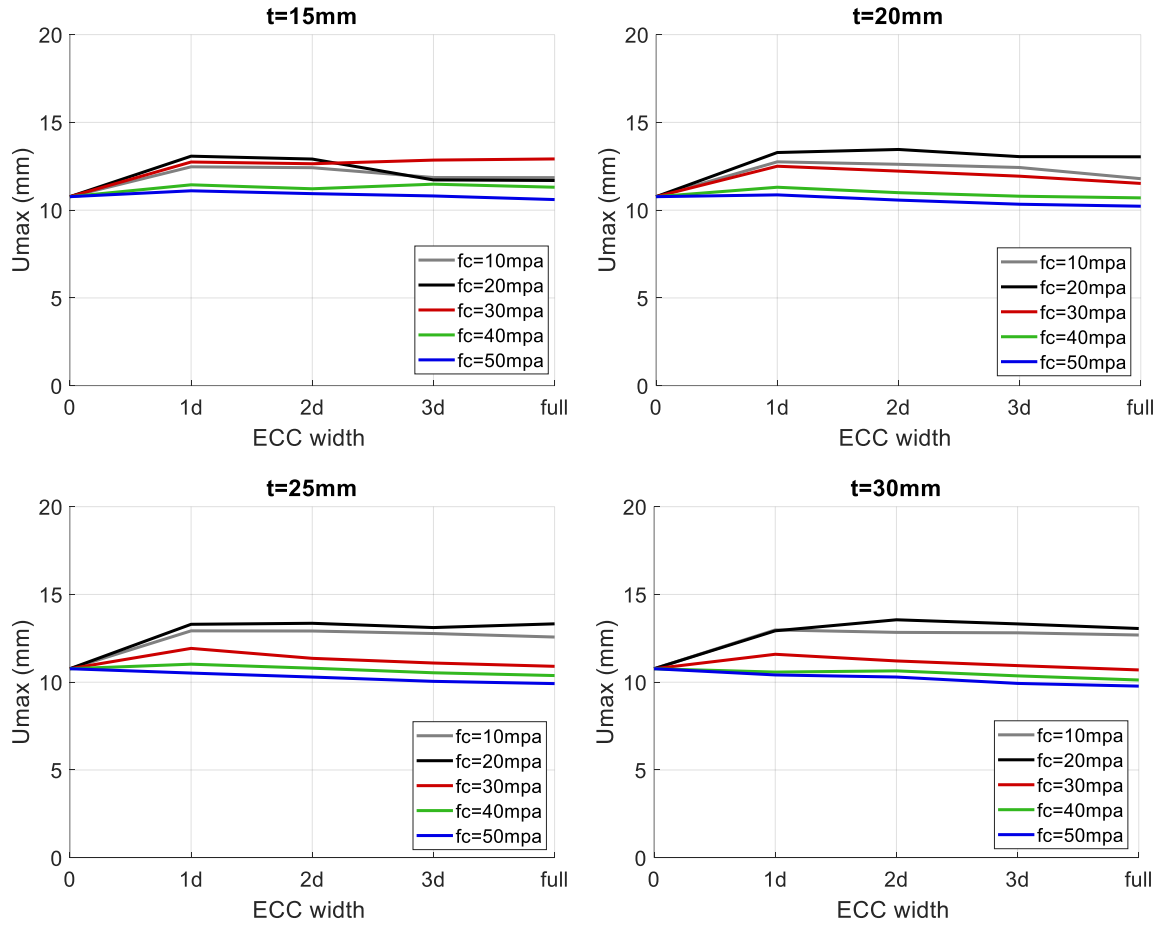

Figure 4.30. Deformation capacity of flat plate for different ECC strengths and widths with thicknesses of 15mm; 20mm; 25mm; and 30mm.

4.4.2. Effect of ECC parameters on tension side retrofitting

Figure 4.31 presents the parametric plot for the peak strengths of flat plates retrofitted on the tension side for varying ECC strengths and widths with thicknesses of 15mm, 20mm, 25mm, and 30mm. Overall, it is clear that the peak strengths of the flat plate with tension side

retrofitting increase only when the 3d or full slab width ECC is applied, indicating that the critical shear perimeter is more than 2d. Furthermore, the strength of flat plates rises with an increase in compressive strength and thickness of ECC. A rise in peak strength ranges from 2.5% to 13.5 % with the highest strength of 867.58 kN obtained for the flat plate model with 30mm and 50 MPa ECC with full slab width.

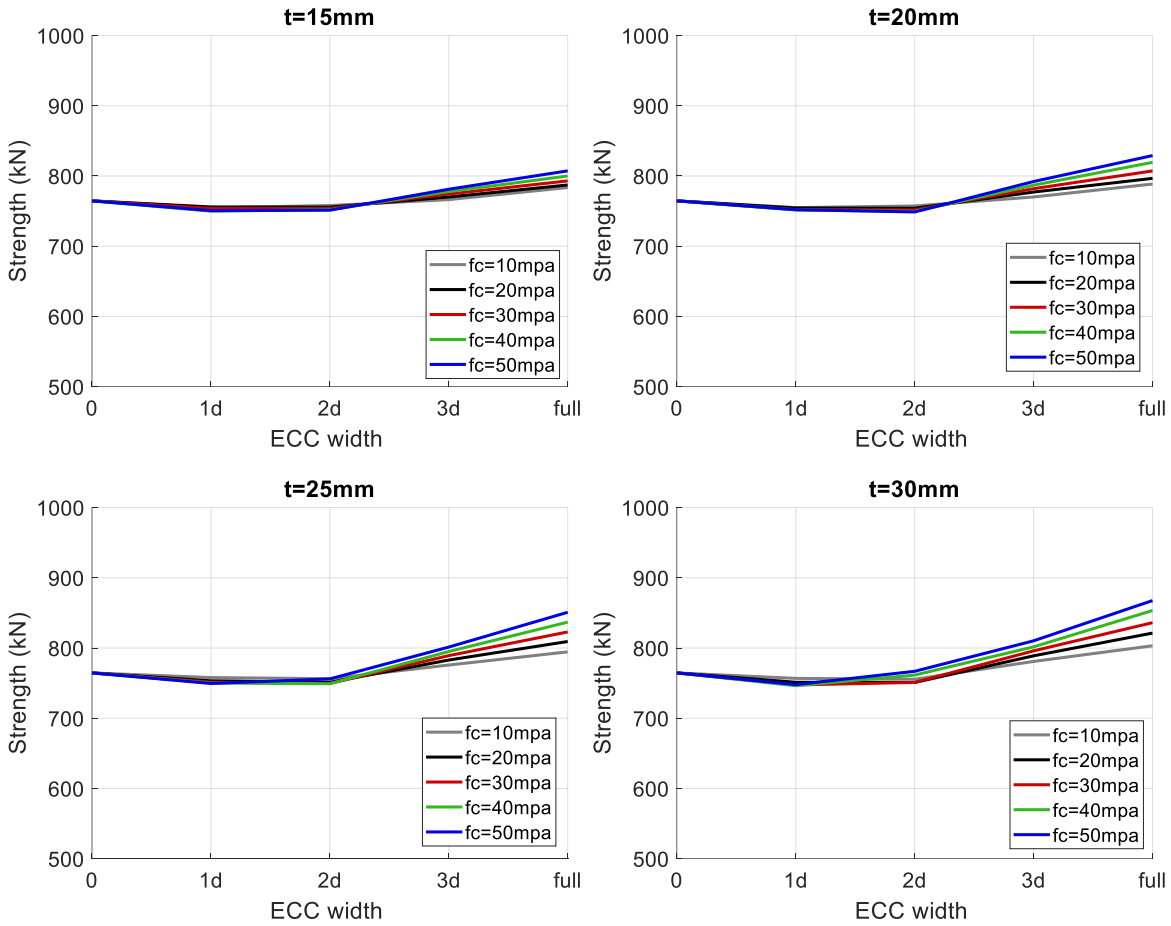

Figure 4.31. Peak strength of flat plate for different ECC strengths and widths with thicknesses of 15mm; 20mm; 25mm; and 30mm.

The deformation capacity plots of flat plates for different ECC strengths and widths with thicknesses of 15mm, 20mm, 25mm, and 30mm are illustrated in Figure 4.32. According to the graphs, the deformation capacity reduces with higher compressive strength and width of ECC. As discussed in the previous section (Section 4.1.2), ECC on the tension side has no direct shear contribution but improves the concrete contribution making it stiffer. Thus, due to the early failure of the concrete, the deformation capacity is reduced. Flat plates with different ECC thicknesses follow the same trend.

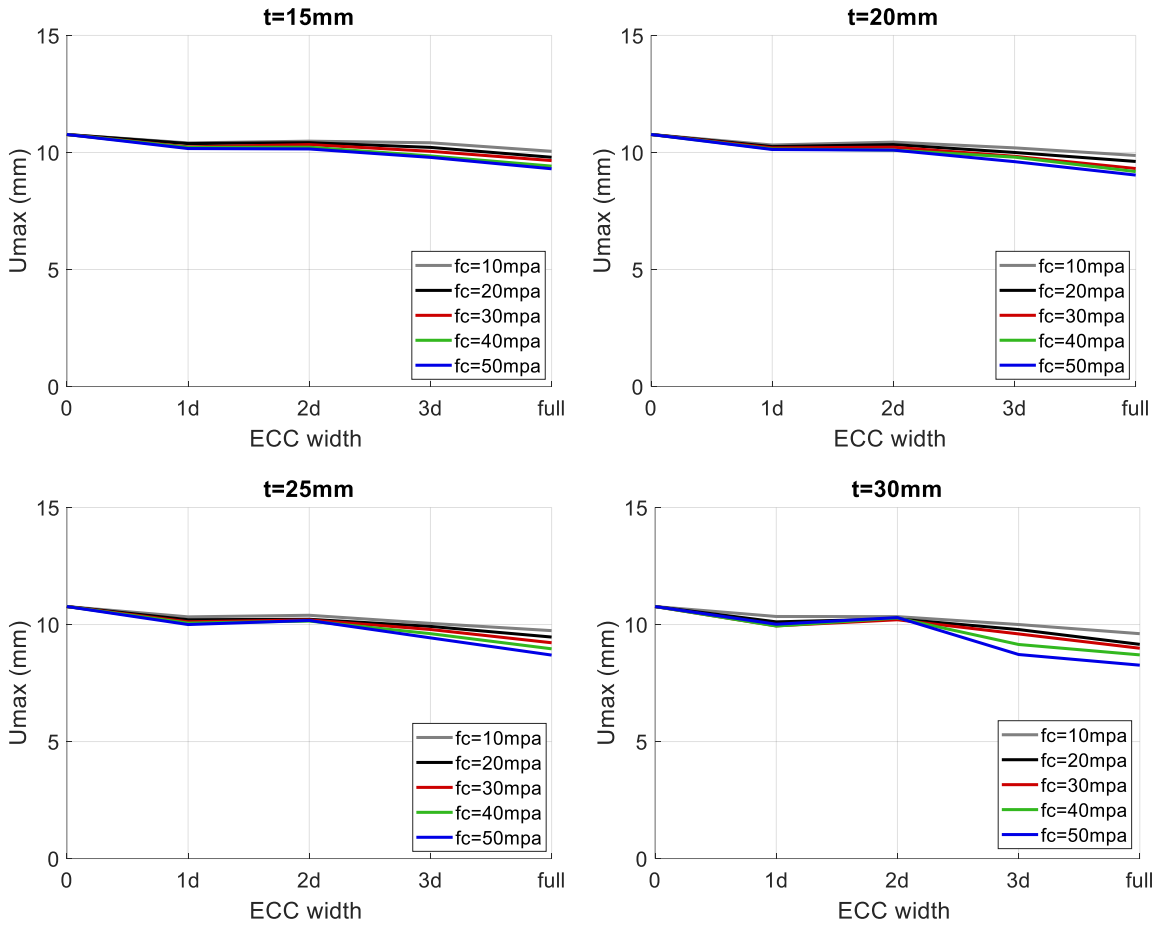

Figure 4.32. Deformation capacity of flat plate for different ECC strengths and widths with thicknesses of 15mm; 20mm; 25mm; and 30mm.

4.4.3. Effect of ECC parameters on double-sided retrofitting

The peak strengths of flat plates retrofitted on both sides for varying ECC strengths and widths with thicknesses of 15mm, 20, 25mm, and 30mm are shown in Figure 4.33. As expected, the double-sided retrofitting considerably enhances the peak strengths of flat plates within the range of 5.6-41.8% increase. The highest strength of 1084.29 kN was obtained for the flat plate model with 30mm and 50 MPa strength ECC applied on the full slab surface. Moreover, it is noted that the higher the strength of ECC, the greater the punching shear strength of flat plates.

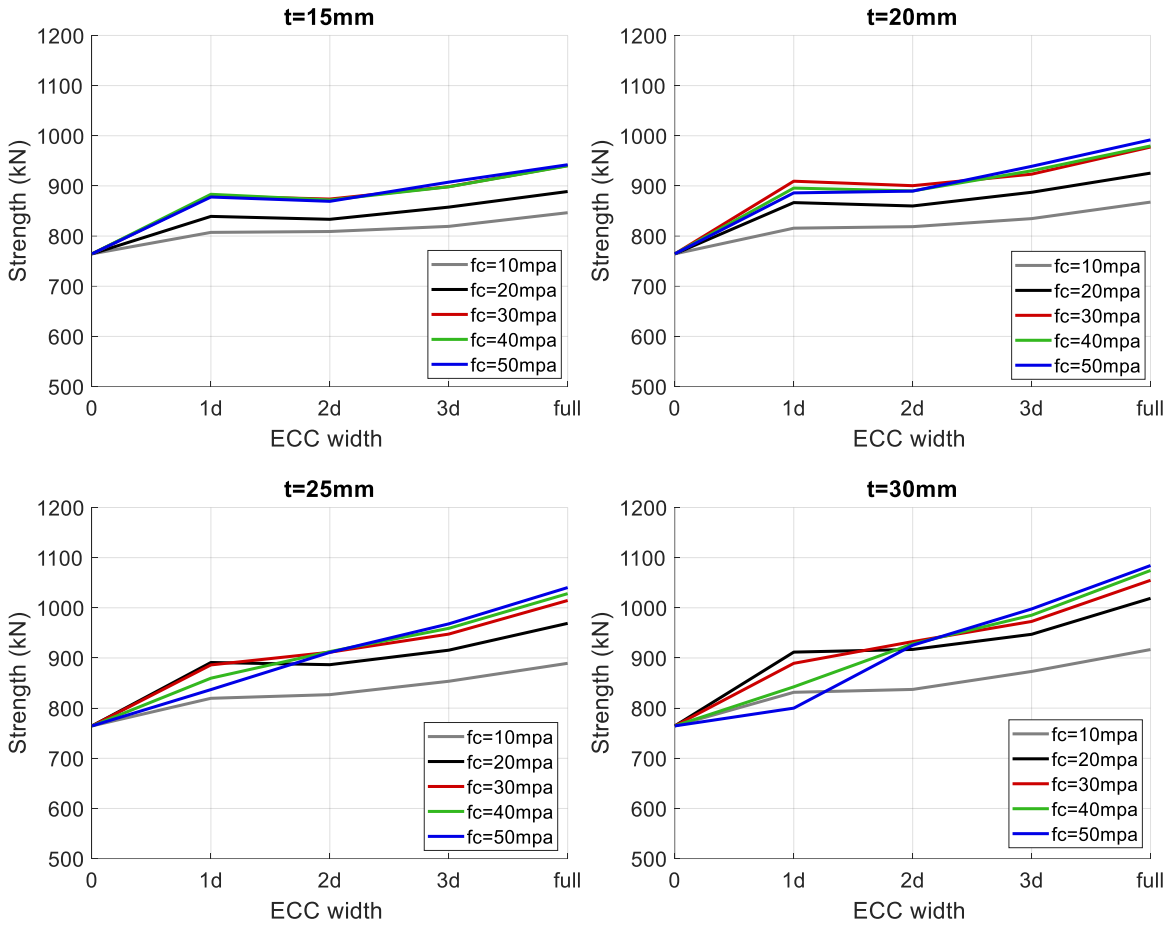

Figure 4.33. Peak strength of flat plate for different ECC strengths and widths with thicknesses of 15mm; 20mm; 25mm; and 30mm.

Figure 4.34 provides the deformation capacity plots for flat plates retrofitted on both sides for varying ECC strengths and widths with thicknesses of 15mm, 20mm, 25mm, and 30mm. Due to the combined contribution of ECC retrofitting from tension and compression sides, the deformation capacity of flat plates is not consistent. The deformation capacity of flat plates with low-strength ECC increases, while normal-strength ECC retrofitted flat plate's deformation capacity reduces.

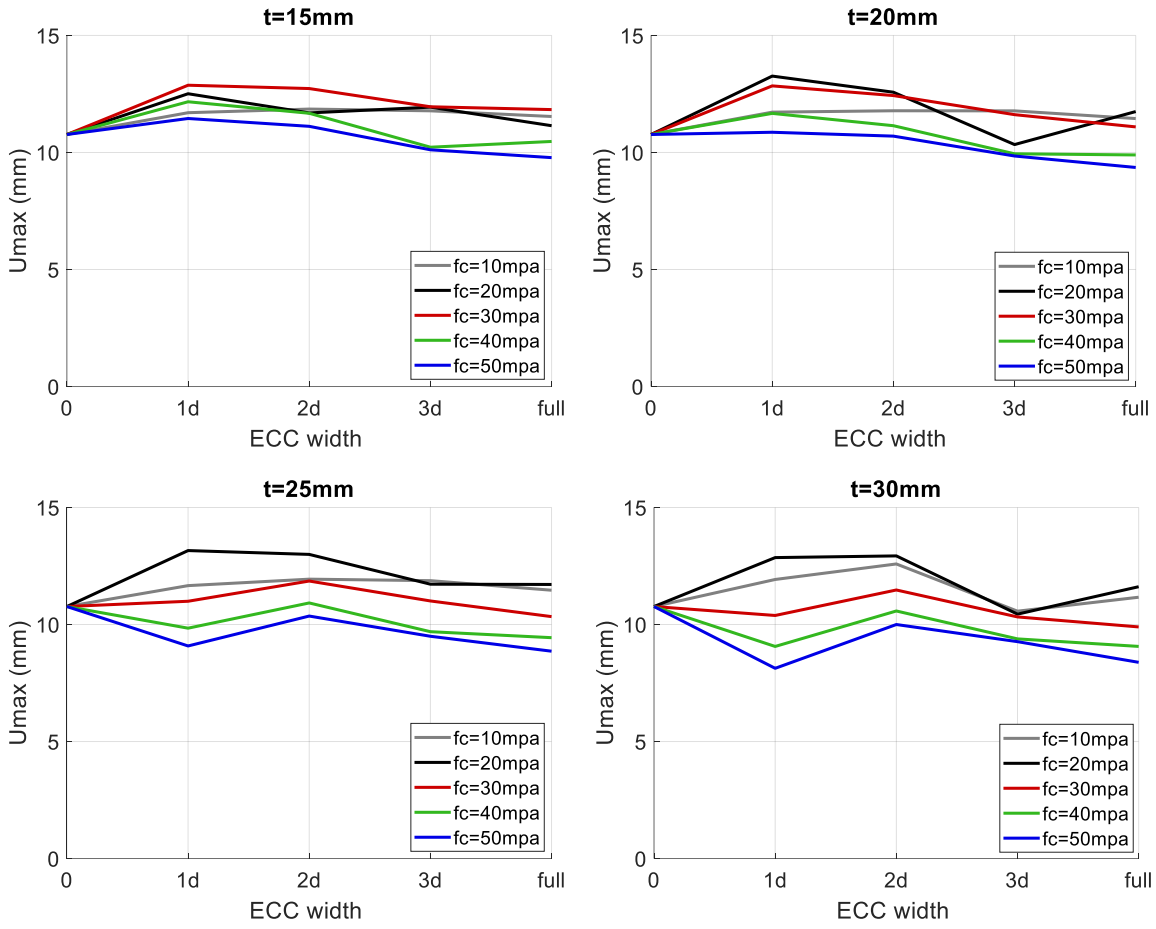

Figure 4.34. Deformation capacity of flat plate for different ECC strengths and widths with thicknesses of 15mm; 20mm; 25mm; and 30mm.

4.4.4. The optimum ECC parameters

Figures 4.35 and 4.36 summarize the parametric study on the punching shear response of flat plates to determine the optimal ECC parameters that can improve the slab-column connection's strength and deformation capacity. According to Figure 4.35a, it is obvious that regardless of the ECC width, the strength of the compression-sided retrofitting remains unchanged. However, when the compressive strength and thickness of ECC increases, the peak strength rise is in the range of 4.64% to 24.26%. The tension side retrofitting results in the lowest strength increase in the range of (-8.44%) to 11.18% and is effective if the width is 3d and full slab width (Figure 4.35b). The double-sided strengthening generates the highest strength and the larger the width of the ECC layer, ECC thickness, and ECC compressive strength, the higher the strength in the range of 4.64% to 43.87% increase (Figure 4.35c). A similar pattern is observed for the case of misaligned double-sided retrofitting with an increase of 4.64-37.33%, where the compression side ECC width is 1d (Figure 4.35d). According to the

analysis of the shear strength contribution and cracking pattern discussed in the above sections, applying ECC layers on both surfaces of the slab is suggested.

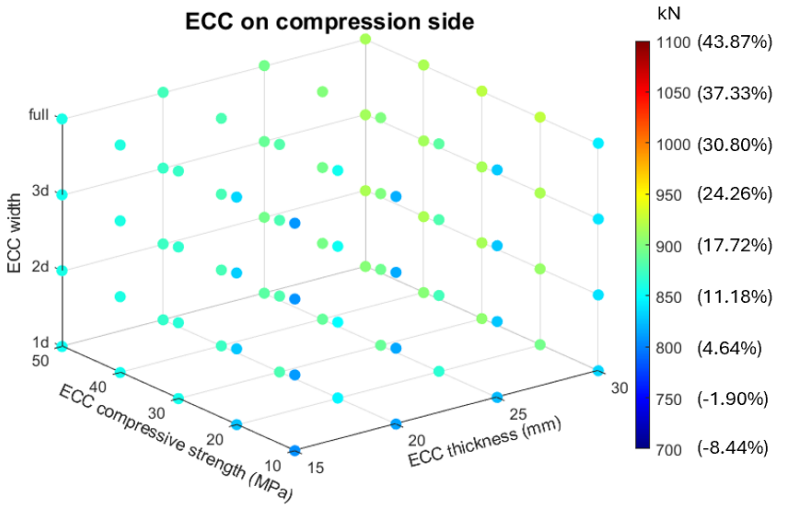

(a)

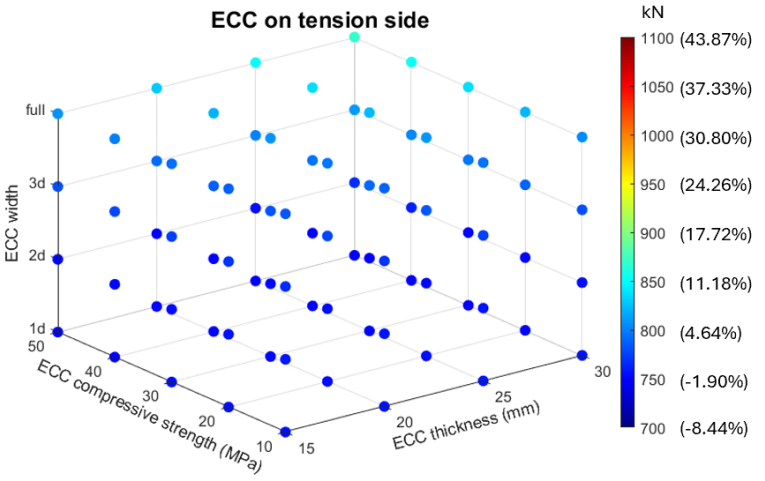

(b)

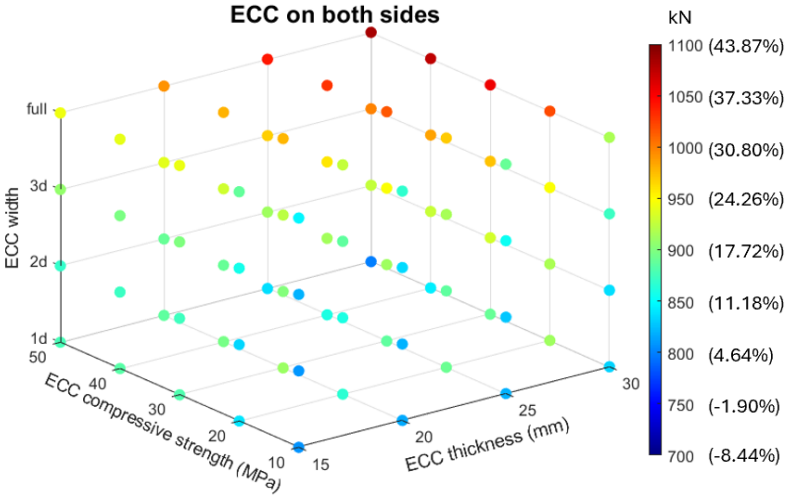

(c)

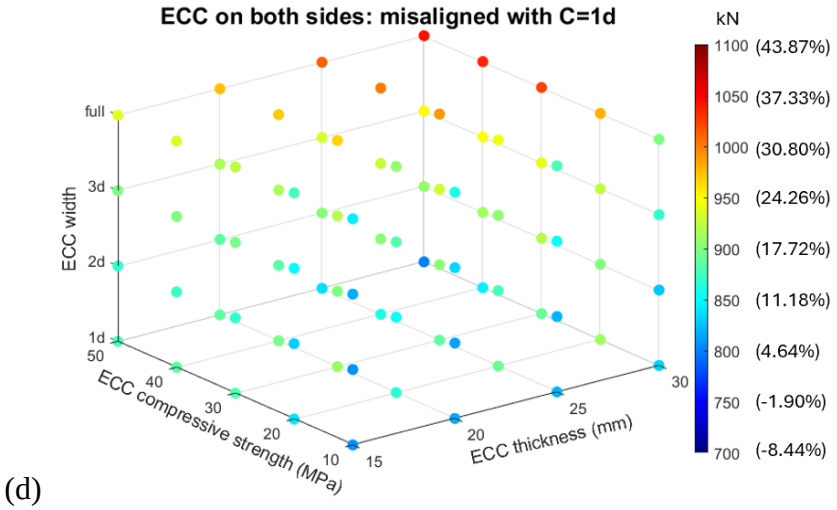

(d)

Figure 4.35. Peak strength of flat plates for different ECC study parameters (a) compression, (b) tension, (c) both, and (d) misaligned retrofitting

According to the deformation capacity (Figure 4.36), flat plates retrofitted with higher compressive strength ECC are more brittle. From Figure 4.36a, it is clear that within the range of low-compressive strength of ECC, flat plates with compression side retrofitting experience the largest deformation capacity increase of almost 30%. However, when the ECC is applied on the tension side, flat plates become stiffer and deformation capacity is reduced by within the range of (-7.14%) to (-25.71%). When the flat plates retrofitted from both sides, the deformation capacity decreases as the compressive strength of ECC increases. The misaligned models provides the similar behavior as the both sided retrofitting. Thus, according to Figure 4.36, it is recommended to employ ECC with compressive strengths up to 30MPa.

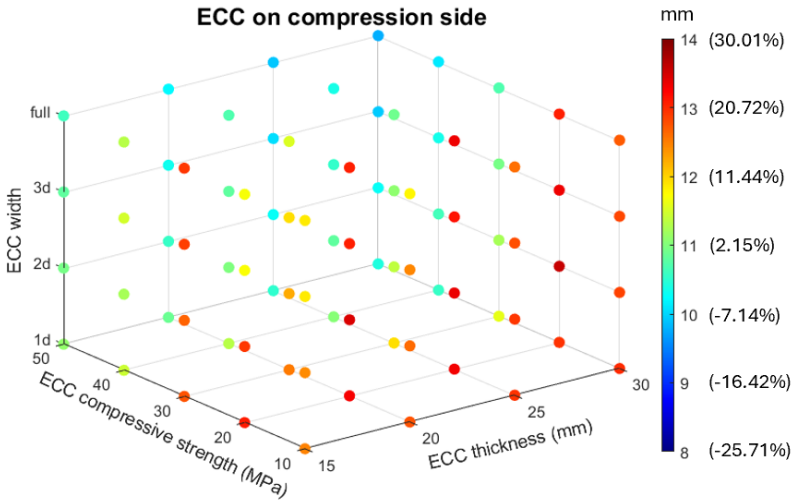

(a)

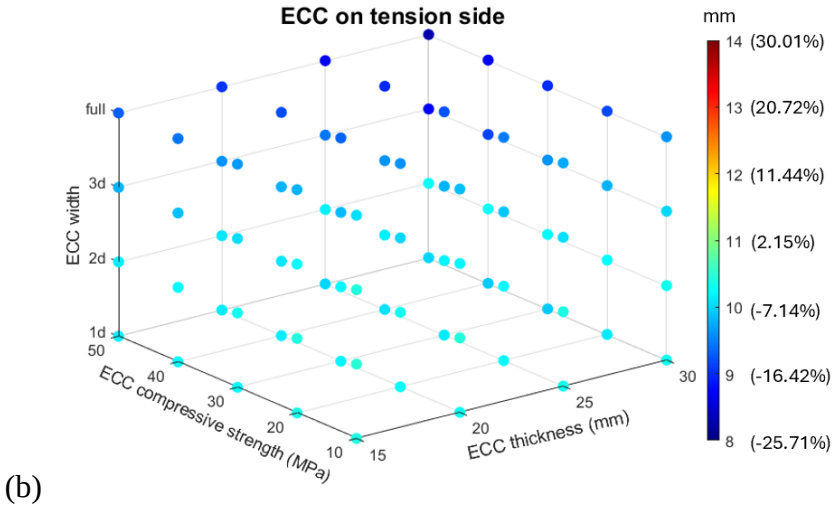

(b)

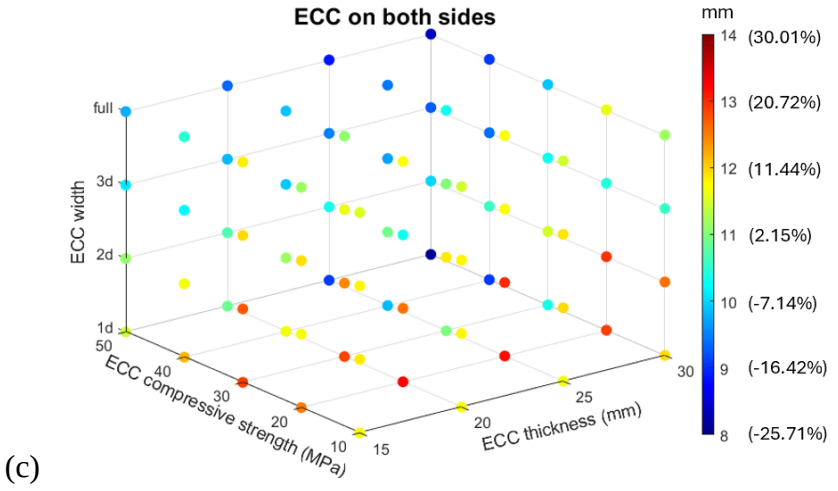

(c)

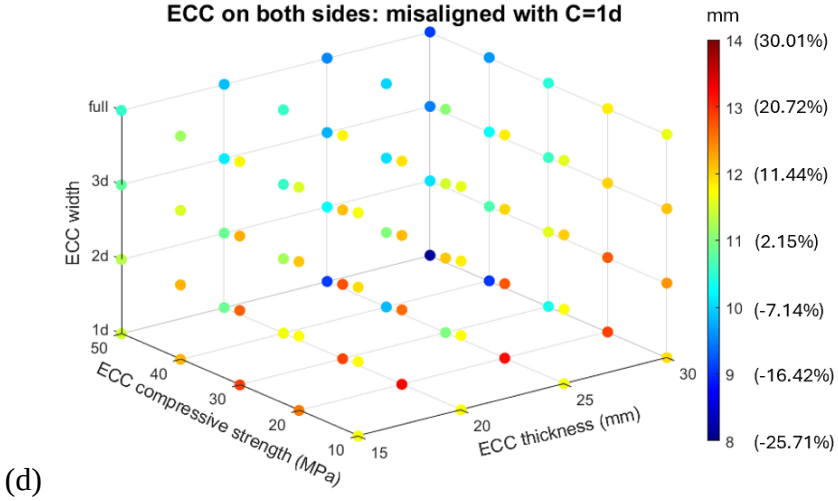

(d)

Figure 4.36. Deformation capacity of flat plates for different ECC study parameters (a) compression, (b) tension, (c) both, and (d) misaligned retrofitting.

Table 4.1 summarizes the optimum ECC parameters that satisfy the deformation capacity development and strength enhancement. In terms of the punching shear strength improvement, double-sided strengthening with full slab width, 50 MPa compressive strength,

and 30 mm thickness ECC is the most effective option with 1084.29kN peak strength, which is 41.82% greater than the unstrengthened model. However, the deformation capacity is significantly low with (-22.14%) decline. The flat plate model that shows the greatest deformation capacity enhancement of 25.89% is the model with 2d width, 20 MPa compressive strength, and 30 mm thickness ECC applied on the compression side of the slab. The most effective option in terms of both strength and deformation capacity is the model with double-sided strengthening with full slab width, 20 MPa compressive strength, and 30 mm thickness ECC, which provides 33.27% and 7.86% increase in strength and deformation capacity, respectively.

Table 4.1. The optimum ECC parameters.

Parameters	Strength	Deformation Capacity	Strength + Deformation Capacity
Location	Both sides	Compression	Both sides
Width	Full	2d	Full
Compressive Strength, MPa	50	20	20
Thickness, mm	30	30	30
Peak strength, kN	1084.29 (+41.82%)	908.12 (+18.78%)	1018.91 (+33.27%)
Deformation Capacity, mm	8.38 (-22.14%)	13.56 (+25.89%)	11.62 (+7.86%)

Chapter 5 – Conclusions

5.1. Conclusion and recommendations

Flat plates are the structural systems widely used due to their simplicity in construction and architectural flexibility. However, the region of the slab-column joint of the flat plate is prone to failure caused by punching shear, which can be described as brittle and severe. Therefore, various retrofitting techniques were studied to prevent punching shear failure. This study focused on the use of engineered cementitious composites as an effective approach to strengthen the slab. For that purpose, the numerical simulations were carried out by building a three-dimensional finite element model of a flat plate with the addition of an ECC layer on slab surfaces. At first, the analytical model was validated with the experimental test results of the existing study to ensure the accuracy of the predicted results. To investigate the impact of the ECC on the punching shear resistance of the flat plate, a parametric study was performed. The study parameters were the compressive strength, thickness, width, and location of ECC. According to the parametric analysis, the following conclusions are possible:

- The strengthening of the flat plate with ECC significantly improves the punching shear response and deformation capacity.
- The ECC retrofitting on the compression side of the slab considerably enhances the punching shear resistance. However, regardless of the ECC width increase, the shear capacity of the slab remains constant.
- The ECC retrofitting on the compression face of the slab with low strength can increase connections' capacity to withstand deformation.
- The ECC retrofitting on the slab's tension side has no direct shear contribution to punching shear failure strength. However, the addition of an ECC layer enhances the contribution of concrete, thus, improving the global response of the flat plate.
- The ECC retrofitting on the slab's tension side is effective in reducing the damaged area of the slab on the tension surface.
- The ECC retrofitting on the tension side of the slab is only effective if the width is 3d or greater.
- The double-sided ECC retrofitting demonstrates the highest punching shear strength and deformation capacity by the effect of the combined contribution of ECC from the compression and tension sides.
- The larger the thickness of ECC, the higher the strength of slab-column assemblage.

Based on the parametric study results, both compression side and tension side retrofitting are crucial to improving the punching shear response of flat plates in terms of strength and deformation capacity. Therefore, double-sided retrofitting with low-strength ECC results in better performance under punching load. Accordingly, it is concluded that in terms of both strength and deformation capacity improvement, the optimum ECC parameters are 20 MPa compressive strength, 30 mm thickness, and full slab width located on both surfaces of the flat plate.

5.2. Limitations and future work

There are several limitations of this study. This thesis work examines only four study parameters. Other parameters including ECC fiber content, ECC layout, flat plate dimensions, and loading conditions can be investigated in future studies. Furthermore, this study investigates only the interior connection of the slab-column assemblage subjected to concentric load. The exterior joints and knee joints can be evaluated in future work to investigate the effect of eccentricity and imbalanced moments. Also, the interior joints under unbalanced moments can be investigated in future studies. Moreover, this study only conducted simulations with flat plates subjected to monotonic loading. The cyclic analyses can be conducted in further work to investigate the behavior of ECC retrofitting for flat plates under seismic conditions.

References

[1] N. J. Gardner, J. Huh, and L. Chung, “Lessons from the Sampoong department store collapse,” Cem Concr Compos, vol. 24, no. 6, pp. 523–529, Dec. 2002, doi: 10.1016/S0958-9465(01)00068-3.

[2] D. Mitchell, R. H. Devall, M. Saatcioglu, R. Simpson, R. Tinawi, and R. Tremblay, “Damage to concrete structures due to the 1994 Northridge earthquake,” Canadian Journal of Civil Engineering, vol. 22, no. 2, pp. 361–377, 1995, doi: 10.1139/l95-047.

[3] I. N. Robertson, “Cyclic Testing of Slab-Column Connections with Shear Reinforcement.” [Online]. Available: https://www.researchgate.net/publication/272682360

[4] U. Prawatwong, P. Warnitchai, and C.H. Tandian, “Seismic Performance of Bonded Post-Tensioned Slab-Column Connections with and without Drop Panels”, Advances in Structural Engineering, vol. 15, no. 10, pp. 1653-1672, 2011.

[5] S. Megally, and A. Ghali, “Punching Shear Design of Earthquake-Resistant Slab-Column Connections,” ACI Structural Journal, vol. 97, no. 5, pp. 720-730, 2000.

[6] H. M. Afefy and E. T. M. El-Tony, “Punching shear resistance of strengthened reinforced concrete interior slab–column connections using ultra-high-performance strain-hardening cementitious composite material,” Advances in Structural Engineering, vol. 22, no. 8, pp. 1799–1816, Jun. 2019, doi: 10.1177/1369433218823841.

[7] M. Amiri, and M.R. Esfahani, “Effect of using Engineered Cementitious Composites (ECC) on failure behavior of flat slab-column connections,” Structures, vol. 47, pp. 2397-2407, 2023, https://doi.org/10.1016/j.istruc.2022.12.058.

[8] I. A. E. M. Shehata and P. E. Regan, “Punching in R.C. Slabs,” *Journal of Structural Engineering*, vol. 115, no. 7, pp. 1726–1740, Jul. 1989, doi: 10.1061/(ASCE)0733-9445(1989)115:7(1726).

[9] I. A. E. M. Shehata, “Simplified model for estimating the punching resistance of reinforced concrete slabs,” *Materials and Structures*, vol. 23, pp. 364–371, 1990.

[10] Ph. Menétrey, “Synthesis of punching failure in reinforced concrete,” Cem Concr Compos, vol. 24, no. 6, pp. 497–507, Dec. 2002, doi: 10.1016/S0958-9465(01)00066-X.

[11] D. D. Theodorakopoulos and R. N. Swamy, “Ultimate punching shear strength analysis of slab-column connections,” Cement & Concrete Composites, vol. 24, pp. 509–521, 2002.

[12] S. D. B. Alexander and S. H. Simmonds, “Ultimate Strength of Slab-Column Connections I,” *ACI Struct J*, vol. 84, no. 3, pp. 255–261, 1987.

[13] ACI Committee 318, American Concrete Institute and International Organization for Standardization, Building code requirements for structural concrete (ACI 318-08) and commentary. American Concrete Institute, 2008.

[14] “EN 1992-1-1: Eurocode 2: Design of concrete structures - Part 1-1: General rules and rules for buildings,” 2004.

[15] Joint ACI-ASCE Committee 421. and American Concrete Institute., Guide to design of reinforced two-way slab systems. American Concrete Institute, 2015.

[16] SP RK 2.03-30-2017. (2018). Construction in Seismic Zones. Astana, AO KazNIISA.

[17] W. Bu, and M. A. Polak, “Seismic Retrofit of Reinforced concrete Slab Connections Using Shear Bolts,” ACI Structural Journal, vol. 106, no. 4, pp. 514-522, 2009.

[18] H.R. Taresh, M.Y.M. Yatim, M.R. Azmi, “Punching shear behavior of interior slab-column connections strengthened by steel angle plates”, Engineering Structures, vol. 238, March 2021, https://doi.org/10.1016/j.engstruct.2021.112246.

[19] K. Sissakis, and S. A. Sheikh, “Strengthening Concrete Slabs for Punching Shear with Carbon Fiber-Reinforced Polymer Laminates,” ACI Structural Journal, vol. 104, no. 1, pp. 49-59, 2007.

[20] Y.J. Kim, J.M. Longworth, R.G. Wight, and M.F. Green, “Punching Shear of Two-way Slabs Retrofitted with Prestressed or Non-prestresses or Non-prestressed CFRP Sheets”, Journal of Reinforced Plastics and Composites, Vol. 29, No. 8, pp. 1206-1223, 2010, DOI: 10.1177/0731684409103143

[21] V. C. Li, “Engineered Cementitious Composites (ECC)-Material, Structural, and Durability Performance,” 2007.

[22] A. Kadhim, H. Alhussainawe, F. H. Arna’ot, A. A. Abbass, and M. Ozakca, “Size Effect on Punching Shear Behavior of Slab-Column Assembly Made From Engineering Cementitious Composite Materials with Polyvinyl Alcohol Fibers,” The International Journal of Energy & Engineering Sciences, pp. 31-40, n.d.

[23] B. Ye, P. Pan, G. Xiao, Y. Zhang, and Z. He, “Experimental investigation on failure modes of RECC slab-column connections under concentric gravity loading,” Eng Struct, vol. 230, Mar. 2021, doi: 10.1016/j.engstruct.2020.111559.

[24] A. Muttoni and J. Schwartz, “Behavior of Beams and Punching in Slabs without Shear Reinforcement,” *In IABSE Colloquium*, vol. 62. pp. 703–708, 1991.

[25] A. Muttoni, “Punching Shear Strength of Reinforced Concrete Slabs without Transverse Reinforcement,” ACI Struct J, vol. 105, no. 4, pp. 440-450, 2008.

[26] ABAQUS (2010) ABAQUS Analysis User’s Manual (Version 6.6). Providence, RI: Dassault Systems SIMULIA Corporation.

[27] A. S. Genikomsou and M. A. Polak, “Finite element analysis of punching shear of concrete slabs using damaged plasticity model in ABAQUS,” Eng Struct, vol. 98, pp. 38–48, Sep. 2015, doi: 10.1016/j.engstruct.2015.04.016.

[28] E. Petersson, “Crack Growth and Development of Fracture Zones in Plain Concrete and Similar Materials”, Doctoral Dissertation, Lund Institute of Technology, Lund, Sweden, 1981.

[29] F. M. Ozkal, “Experimental investigation on the applicability of the geogrid: Comparison between conventional and hybrid-reinforced irregular reinforced concrete members”, Advances in structural engineering, June 2021, https://doi.org/10.1177/1369433218786045.

[30] Md. I. Kabir, C.K. Lee, M.M. Rana, and Y.X. Zhang, “Flexural and Bond-slip Behaviours of Engineered Cementitious Composites Encased Steel Composite Beams”, Journal of Constructional Steel Research, vol. 157, pp. 229-244, 2019, https://doi.org/10.1016/j.jcsr.2019.02.032.